phospho-PERK (980Thr), anti-phopsho-eIF2α (51Ser), and (**B**) MIN6 cells were treated with either control 0.5% BSA or 400 μM palmitate+0.5% BSA at a concentration of 5, 10, 25 mM glucose for 18 hours and blotted with anti-ATF3 and anti-CHOP antibodies. β-Actin was detected for loading control. Tunicamycin treatment was control for ER stress. (**C**) Cells were treated with either 500 μg/ml NaCl (ionic control) or 500 μg/ml TUDCA 15-h prior to beginning of palmitate treatment and then were co-treated with either 0.5% BSA or 400 μM palmitate+0.5% BSA with either 5 mM or 25 mM glucose and NaCl or TUDCA for 24 h. Total cell lysates were subjected to Western blot analysis with antibodies to the indicated proteins. Densitometry of total CHOP and cleaved Caspase3 and Pdx1 were measured and normalized over α-Tubulin, respectively. Densitometry of phospho-cJun was measured and normalized over total JNK. The representative results of three individual experiments are shown. The effects on CHOP, cleaved Caspase3 and phospho-cJun and Pdx1 protein are graphically illustrated. *$p<0.05$. (**D**) Cells were treated with either 500 μg/ml NaCl (ionic control) or 500 μg/ml TUDCA 15-h prior to beginning of palmitate treatment and then were co-treated with either 0.5% BSA or 400 μM palmitate+0.5% BSA with either 5 mM, 10 mM or 25 mM glucose and NaCl or TUDCA for 24-h. Total cell lysates were subjected to Western blot analysis with antibodies to the indicated proteins. Densitometry of total IRS2 was measured and normalized over α-Tubulin and densitometry of phospho-Akt was measured and normalized over total Akt. The representative results of three individual experiments are shown. The effects on IRS2 protein are graphically illustrated, *$p<0.05$, **$p<0.01$.
doi:10.1371/journal.pone.0018146.g003

shRNA adenovirus constructs described previously [14] were incubated with the cells at an MOI of 30 for 4 hours in normal culture media. Palmitate and cytokine treatments were initiated 24 hours following removal of virus.

Inhibition of Gsk3β expression with a kinase dead adenovirus

Adenovirus expressing a catalytic inactive mutant of the human Gsk3β (Adv-Gsk3βKM) was prepared as previously described [21]. Control adenovirus-green fluorescent protein (AdV-GFP) was a gift from D. Kelly (Washington University, St. Louis, MO). Infection of the MIN6 cells was carried out at the indicated multiplicity of infection (MOI) for one hour in serum-free media. The MIN6 were then washed in PBS, maintained in the DMEM/15% FBS media, and then experiments were carried out 24 hours after infection.

Statistical analysis

The presented data were analyzed from at least 3 independent experiments and are shown as means ±S.E.M. The significance of the variations was analyzed using either a one- or two-way ANOVA with Bonferroni corrections with a significance level of 0.05 (95% confidence intervals).

Results

Glucose and palmitate synergize to induce apoptosis

Our previous study had shown a dose-dependent effect of FFA, both palmitate (50–400 μM) and oleate (50–400 μM), on ER stress and apoptosis in glucose-responsive insulinoma (MIN6) cells [16]. In the current study the dose-dependent effect of glucose (5–25 mM) was examined at 400 μM palmitate. As shown in Figure 1A, increasing glucose concentration had a clear synergistic effect on cell death characterized by propidium iodide incorporation normalized to DAPI staining. While 400 μM palmitate resulted in about 3% propidium iodide incorporation at 5 mM glucose, this was increased more than threefold when the glucose concentration was raised to 15 mM and 25 mM. While there was no effect of palmitate on cleaved Caspase3 at 5 mM glucose, consistent with the synergism observed on propidium iodide staining, glucose and palmitate also synergized on activation of the pro-apoptotic marker cleaved Caspase3 comparing that at 5 mM glucose/palmitate vs. 25 mM glucose/palmitate, $p<0.05$ (Figure 1B).

We next explored the underlying mechanisms for the glucose potentiation. FFA treatment has been shown to induce JNK activation that can contribute to FFA-induced apoptosis; we determined the effects of altering glucose concentrations on JNK activation. Interestingly, JNK activation by FFA was maximal at the lowest glucose concentration and did not increase further as glucose was increased (Figure 1B). Maximal FFA activation of JNK at 5 mM glucose with apparent increasing activation of cleaved Caspase3 with increasing glucose concentration suggested that further enhancement of JNK by glucose could not explain the synergistic effects on cell death.

Glucose and palmitate synergize to reduce insulin signaling associated with a decrease in IRS2 protein

Previous studies have shown that glucose treatment of insulinoma cells results in activation of the insulin receptor substrate-PI3-kinase-Akt pathway that serves to protect against β-cell death. In contrast, FFA treatment of insulinoma cells inhibits this pathway [8,16]. We examined whether the synergistic effect of glucose on FFA-induced apoptosis could be related to inhibition of this signaling pathway. Glucose alone (5–25 mM), as shown in the first four lanes of Figure 2, increased phospho-Akt (S473) and phospho-Gsk3 as expected, with no apparent change in IRS1 or IRS2 proteins, confirming previous observations [8,22]. However as glucose was raised in the presence of palmitate (Figure 2, lanes 5–8) a dose-dependent decrease in phospho-Akt and phospho-Gsk3β were observed and accompanied by a parallel decrease in IRS2, while IRS1 levels did not appear to change. This synergistic effect of increasing glucose in the presence of FFA on inhibition of IRS2 and PI-3 kinase-Akt signaling is a novel finding that might explain the synergistic effect on β-cell survival [23].

The effect of glucose and FFA is accompanied by a synergistic effect on ER stress that is reduced by addition of a chemical chaperone

FFA impair insulin signaling in β-cells in part via activation of ER stress [16,24]. Bachar et. al. [13] recently showed in insulinoma cells that palmitate at 22.2 mM glucose vs. 3.3 mM glucose increased activation of JNK, CHOP and the ER stress enzyme phospho-PERK. We examined the effects of increasing glucose from 5 mM to 25 mM at 8 and 18 hours of treatment to observe the different time course of development of ER stress markers. An enhancement of the ER stress markers phospho-PERK, phospho-eIF2α, CHOP, and ATF3 (Figure 3A and 3B) was observed, confirming and extending the results of Bachar et. al. [13]. The observation that glucose appeared to synergize with palmitate to increase ATF3 protein expression, although this was not statistically significant, was consistent with the previous finding by Hartman et. al. demonstrating that high glucose and FFA together increased ATF3 mRNA expression, and that this was associated with increased apoptosis of insulinoma cells [25]. These glucose-induced changes in the presence of palmitate on ER stress markers were again noted in the absence of phospho-c-Jun (Figure 3C).

We next examined whether reducing ER stress using TUDCA, a chemical chaperone that enhances ER functional capacity [26],

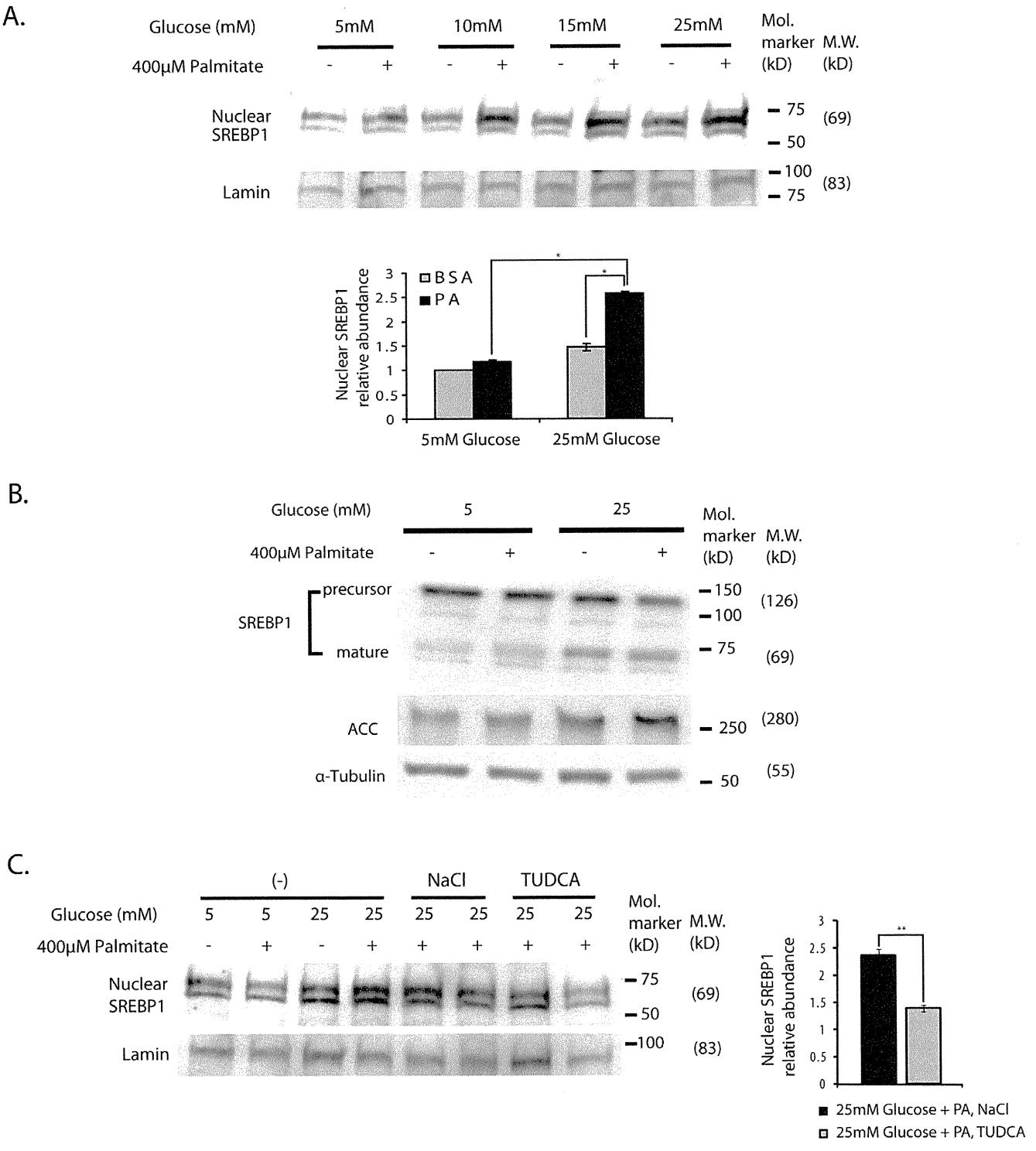

Figure 4. The synergistic effects of glucose and palmitate on ER stress results in concomitant effects on activation of SREBP1. (**A**) MIN6 cells were treated with either control 0.5% BSA or 400 μM palmitate+0.5% BSA at a concentration of 5, 10, 15, 25 mM glucose for 18-h. Nuclear fractions were extracted from the cells and were subjected to Western blot analyses using anti-SREBP1 and anti-Lamin antibodies. 25 μg of nuclear protein was loaded in each lane. The upper band normalized over Lamin was used to do the quantification (the lower band is nonspecific). The relative ratio of nuclear SREBP1 over Lamin calculated by densitometries was summarized as means ± S.E.M. in the graph respectively. The representative results of three experiments are shown, and graphically illustrated, * $p<0.05$. (**B**) MIN6 cells were treated with either control 0.5% BSA or 400 μM palmitate+0.5% BSA at a concentration of either 5 or 25 mM glucose for 24-h. Total cell lysates were subjected to Western blot analysis using anti-acetyl CoA carboxylase (ACC) and anti-α-Tubulin antibodies. The representative results of two individual experiments are shown. (**C**) Cells were treated with either 500 μg/ml NaCl or 500 μg/ml TUDCA 15-h prior to beginning of palmitate treatment. Cells were co-treated with either 0.5% BSA or 400 μM palmitate+0.5% BSA with 25 mM glucose and NaCl or TUDCA for 18-h. Nuclear fractions were extracted from the cells and were subjected to Western blot analyses using anti-SREBP1 and anti-Lamin antibodies. The upper band normalized over Lamin was used to do the quantification (the lower band is nonspecific). 25 μg of nuclear extracts were loaded in each lane. The representative results of three individual

experiments are shown. The relative ratio of nuclear SREBP1 over Lamin calculated by densitometries was summarized as means ± S.E.M. in the graph respectively **p<0.01.
doi:10.1371/journal.pone.0018146.g004

can reverse the synergistic effects of glucose and FFA on insulin receptor substrate signaling. As shown in Figure 3C, the effects of 24 hour treatment with 5 mM or 25 mM glucose in the presence and absence of palmitate (400 μM) on activation of JNK and other markers of ER stress are shown in the control condition with NaCl (first 4 lanes). The results of protein expression under the same conditions but in the presence of TUDCA are shown in the last 4 lanes of Figure 3C. JNK activation, which again was not augmented by the combination of high glucose and palmitate, was little affected by TUDCA treatment. In contrast the other ER stress markers phospho-eIF2α, CHOP and cleaved Caspase 3 were attenuated by co-treatment with TUDCA. Addition of TUDCA also increased Pdx1 (Figure 3C). The increase in phospho-Akt protein levels, an inhibitor of Gsk3 activity, and IRS2 protein levels were also observed with TUDCA treatment (Figure 3D). Together the results suggest that glucose potentiation of FFA induced apoptosis involves activation of ER stress with resultant inhibition of insulin signaling in a manner independent of further JNK activation.

Glucose and palmitate synergistically activate SREBP1

Sterol regulatory element-binding protein-1 (SREBP1) is a transcription factor that stimulates expression of lipid-regulatory genes [27]. SREBP1 is an ER membrane resident protein that in response to sterol depletion is cleaved to generate a transcriptionally active N-terminal fragment that translocates to the nucleus [28]. SREBP1 is increased in liver and islets of diabetic animals [29]. *In vivo* SREBP1 overexpression increased lipid accumulation in islets, reduced β-cell mass, and impaired insulin secretion [30]. Overexpression of the SREBP1 gene in insulinoma and islet β-cells also reduced IRS2 protein [31]. Furthermore, incubation of insulinoma cells and islets with high glucose (25 mM) was shown to activate SREBP1. The latter study examined only high glucose, and did not include FFA. As shown in Figure 4A, like the study of Wang et. al [31] we observed an apparent slight effect of increasing glucose on SREBP1 activation, when nuclear SREBP1 was corrected for nuclear Lamin. A synergistic effect was observed of glucose and FFA on activation of SREBP1 with a concomitant reduction of SREBP1 precursor and appearance of mature or nuclear SREBP1. SREBP1 activation was further confirmed by increased expression of its target acetyl-CoA carboxylase (ACC) (Figure 4B). SREBP1 activation was reduced by attenuation of ER stress with TUDCA pretreatment (Figure 4C) that suggested that the synergistic effects of glucose and palmitate on activation of SREBP1 were mediated by exacerbation of ER stress.

Glucose/palmitate activate ER stress and reduce insulin signaling in primary islets

To validate the relevance of synergistic effects of glucose and palmitate on pancreatic β-cells we treated isolated primary mouse islets with 11 mM or 30 mM glucose in either the absence or presence of 400 μM palmitate for 72 hours. This incubation time and different glucose concentrations were utilized as it was determined that primary islets are more resistant to FFA induced apoptosis than are insulinoma cells (data not shown). Treatment with high glucose (30 mM) and palmitate resulted in an apparent but not significant ($p = 0.14$) enhanced induction of cleaved Caspase3 (Figure 5A), and an apparent but not significant ($p = 0.07$) reduced IRS2 expression (Figure 5B). In addition, high glucose and palmitate synergistically enhanced the ER stress marker GRP78 ($p<0.05$) beyond JNK activation (Figure 5C), and caused an apparent increase in ATF3 ($p = 0.06$) (Figure 5D). Consistent parallel increases in nuclear SREBP1 and total ACC protein also appeared to be potentiated by high glucose and palmitate although the effects were not significant (Figure 5E). Treatment with high glucose and palmitate did however result in significant reduction of phospho-Akt, Pdx1, and phospho-Gsk3b with no change in phospho-cJun (Figure 5F). These data together support the relevance of findings in insulinoma cells to primary islet β-cells.

Loss-of-function of ATF3 and gain-of function of IRS2 reduce the effects of glucose and palmitate on apoptosis

To assess the effects of ER stress-induced ATF3 expression and subsequent suppression of IRS2 on glucolipotoxicity mediated apoptosis, loss- and gain-of-function studies were conducted. INS-r3 cells were utilized as the reagents for small hairpin RNA (shATF3) were controlled for rat ATF3 and not mouse. A similar role for ATF3 in MIN6 and INS1 insulinoma cell stress response has been observed (Zmuda and Hai, unpublished observations). INS-r3 cells were incubated with 400 μM palmitate/25 mM glucose for the indicated times in the presence of adenoviruses expressing either control or shATF3 to reduce ATF3 expression [14]. Note that phospho-Akt appeared to be elevated in cells expressing shATF3 at all times consistent with the known inhibitory effect of ATF3 on IRS2 transcription and subsequent insulin signaling. The IRS2 levels in the ATF3 knockdown cells appeared to be elevated relative to that in control cells at both 8 and 16 hours of glucose/palmitate treatment. Further cleaved Caspase3, following glucose/palmitate treatment, was suppressed in ATF3 knockdown cells ($p<0.002$). The conclusion that ER stress activates ATF3 that contributes to impaired insulin signaling and apoptosis is thus supported by these ATF3 knockdown experiments.

In another experiment using primary islets treated with glucose/palmitate for 72 hours, the effects of transfection with an adenovirus expressing IRS2 was compared to that of islets with control adenovirus. As shown in Figure 6B, where Immunodetection was set to assess high levels of IRS2 in IRS2 transfected cells, there was a marked increase in IRS2 protein with IRS2 overexpression. Glucose/palmitate treatment resulted in increased ATF3 and cleaved Caspase3 with control adenovirus, while overexpression of IRS2 appeared to reduce the degree of apoptosis as measured by reduction of cleaved Caspase3 (Figure 6B). These results are consistent with the previously demonstrated role of ATF3 on ER stress induced apoptosis in islets [14,25].

Loss-of-function of Gsk3β on glucose and palmitate induced β-cell apoptosis

The progressive decline in insulin receptor substrate signaling observed with decreasing IRS2 expression and phospho-Akt was associated with decreased phosphorylation of Gsk3β (Figure 2) and thus activation of the pro-apoptotic form of Gsk3β [32]. To examine the contribution of activation of Gsk3β, the effects of palmitate treatment with increasing amounts of an adenovirus expressing a catalytic inactive mutant of the human Gsk3β (Adv-Gsk-3βKM) were analyzed by Western blot (Figure 7A). A control sample was placed on either end of the blot to facilitate

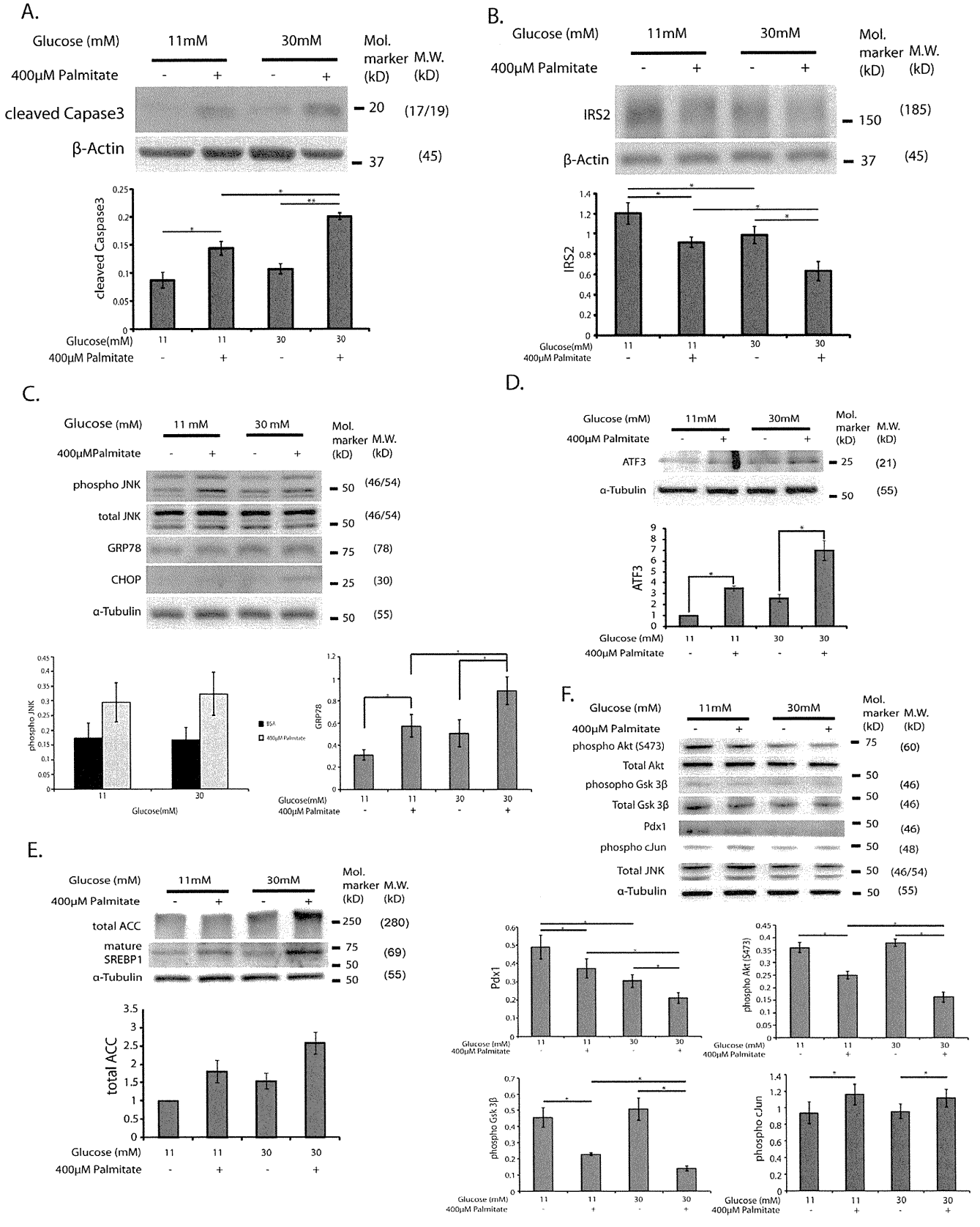

Figure 5. Synergistic effects of glucose and palmitate on ER stress and suppression of IRS2 expression levels in primary mouse islets. Islets from 14 weeks of age C57BL/6 male mice were isolated as described in Methods and were treated with either control 0.5% BSA or 400 μM palmitate+0.5% BSA in RPMI medium containing either 11 mM or 30 mM glucose, 10% FBS for 72-h. Total cell lysates were extracted from

the islets and subjected to Western blot analysis using (**A**) anti-cleaved Caspase3 and anti-β-Actin, (**B**) anti-IRS2 antibodies, (**C**) anti-phospho-JNK, anti-total JNK, anti-GRP78, anti-CHOP, anti-α-Tubulin antibodies, (**D**) anti-ATF3 antibodies, (**E**) anti-Acetyl CoA Carboxylase (ACC), anti-SREBP1, anti-α-Tubulin antibodies, (**F**) anti-Pdx1, anti-phospho-Gsk3β, anti-total Gsk3β, anti-phospho-Akt (S473), anti-phospho-cJun, anti-α-Tubulin antibodies. The blots shown are representative of 3 individual islet experiments. The relative ratio of indicated protein over β-Actin or α-Tubulin as a loading control calculated by densitometries was summarized as means ± S.E.M. in the graph respectively *$p<0.05$, **$p<0.01$.
doi:10.1371/journal.pone.0018146.g005

comparisons. For instance, observe the increase in cleaved Caspase3 and phopho-JNK between the two controls on either end of the blot. Increasing doses of the virus correlated with increased levels of total Gsk-3β, and reduced levels of the Gsk-3β substrate phospho-GS. Increased kinase dead Gsk-3β virus also resulted in increased expression of Pdx1, reduced apoptosis as suggested by cleaved Caspase 3 levels, and cell death measured by propidium iodide incorporation (Figure 7B). Interestingly the protective effects of the Adv-Gsk-3βKM occurred in spite of apparent comparable activation of phospho-JNK with palmitate treatment.

Discussion

The combination of hyperglycemia and hyperlipidemia that is associated with insulin resistance may contribute to reducing β-cell mass and promoting the transition to full blown Type 2 diabetes, but the underlying mechanisms are only partially understood. This study examined the sequence of molecular events that may be involved in this process, and resulted in several novel observations: 1) While early induction of JNK plays a role in FFA-induced apoptosis [13,16], it does not appear involved in the high glucose potentiation of FFA effects; 2) the potentiating effects of glucose and FFA on ER stress result in activation of ER-associated SREBP1 and ATF3 leading to reduced IRS2 expression further impairing insulin-receptor substrate-PI-3K-Akt signaling, and 3) treatment with an adenovirus expressing a kinase dead Gsk3β significantly restored Pdx1 levels, and reduced the apoptosis induced by high glucose and FFA. Together these findings provide a molecular model for the synergistic effects of glucose and FFA on islet cell death and identify potentially useful therapeutic targets.

The role of JNK activation in FFA-induction of apoptosis in β-cells has been documented [13,16,33]. In the current study, JNK activation by palmitate was significant as expected, but was maximal at low glucose, and glucose potentiation of FFA-induced apoptosis was JNK independent (Figure 1B). How FFA treatment of β-cells leads to JNK activation is not completely known, but FFA induce ER stress, which activates JNK activation, and JNK activation itself can induce ER stress [13,34]. Interestingly, TUDCA appeared to reduce cleaved Caspase3 and CHOP induction, while not appearing to reduce JNK activation (Figure 3) suggesting that in this case JNK activation is upstream of ER stress. On the other hand the results of inhibition of ATF3 by shRNA in Figure 6A suggest that JNK activation is upstream of ER stress. Our results do not therefore settle this issue of the relative position of JNK activation and ER stress. Regardless of whether JNK activation is upstream or downstream of ER stress, the findings in the current study show that the combination of high glucose and FFA does not associate with further activation of JNK as compared to FFA in low glucose. This result is to some extent in conflict with that of Bachar et. al. [13] who showed that incubating islet cells in low vs. high glucose resulted in both increased ER stress and JNK activation. A difference in the two experiments is that Bachar et.al. evaluated islet cells in 3.3 mM vs. 22 mM glucose, and our experiments assessed cells in 5.5 mM vs. 25 mM glucose. Our results do not rule out the contributory effect of JNK on β-cell apoptosis as previously shown [13,16,33] but they emphasize the importance of additional mechanisms contributed by high glucose. Additionally, since glucose and palmitate have been shown to evoke oxidative stress, impairing nuclear translocation of Pdx1 and triggering β-cell failure [35], it is conceivable that oxidative stress interacts with JNK, ATF3 and ER stress to contribute to glucose/palmitate induced apoptosis, although this hypothesis remains to be tested.

The role of SREBP1 in high glucose induced apoptosis in islet β-cells has been reported [31]. In the absence of FFA, high glucose alone for 48 hours was shown to activate SREBP1 and to repress IRS2 and Pdx1 levels. Expression of a dominant negative SREBP1 reversed these transcriptional effects. In the current study, glucose alone at high concentration slightly activated SREBP1 as shown in Figure 4, an event that did not correlate with ER stress or apoptosis. A much more significant activation of SREBP1 was observed with glucose and palmitate together and this was shown to be a function of induced ER stress since it was attenuated by TUDCA (Figure 4C). These results only show an association of SREBP1 nuclear translocation, and do not document its causal role. It is likely however that SREBP1 nuclear translocation participates in glucose/palmitate induced apoptosis, as previous studies documented the causal role of SREBP1 in ER stress induced apoptosis in insulinoma cells [31]. SREBP1 resides in the ER membrane, where it is anchored by the labile protein INSIG1 [36]. The link between ER stress and SREBP1 activation has been little studied. Lee et. al. using CHO cells [36] showed that thapsigargin, a chemical that induces ER stress, activates SREBP1 due to rapid degradation of INSIG1 [36]. We observed that glucose and palmitate together appeared to reduce INSIG1 protein (data not shown), which likely contributed to augmentation of nuclear SREBP1 under these conditions.

Similarly a synergistic effect of glucose and FFA was observed on expression of the ER-associated stress marker ATF3. ATF3 expression paralleled suppression of IRS2 protein levels, and induction of apoptosis measured by CHOP (Figure 3A–B), and Caspase3 activation (Figure 3A). The association of ATF3 with ER stress and cell death has been well documented [37] but there is relatively little known related to ATF3 targets [14]. Recently, ATF3 was shown to suppress the IRS2 protein by binding to the IRS2 promoter [14] and implicated this mechanism in apoptosis induced by agents such as γ-interferon, TNF-α, or thapsigargin. Our findings are consistent with the involvement of ATF3 in the apoptotic effects of nutrient induced ER stress in islet cells. In this context, we note that Cunha et. al. [33] did not find a pro-apoptotic role of ATF3 in the context of palmitate treatment. Potential explanations for this apparent difference include the difference in glucose concentration (25 mM glucose in our study and 11 mM glucose in theirs), the cells used (INS-r3 in our study and INS-1E in theirs), and assays (activated Caspase3 in our study and propidium iodide plus Hoechst stain). An interesting question is whether ATF3 is a direct repressor of Pdx1 expression. Insulin signaling alters Gsk3β and FoxO activity [16,32,38,39] and these proteins are known regulators of Pdx1 expression. As ATF3 represses IRS2 and insulin signaling, at least part of ER stress and ATF3 induced Pdx1 suppression is due to decreased insulin signaling, and perhaps also due to direct suppression of Pdx1 expression, but this latter question remains to be determined by future experiments. Interestingly

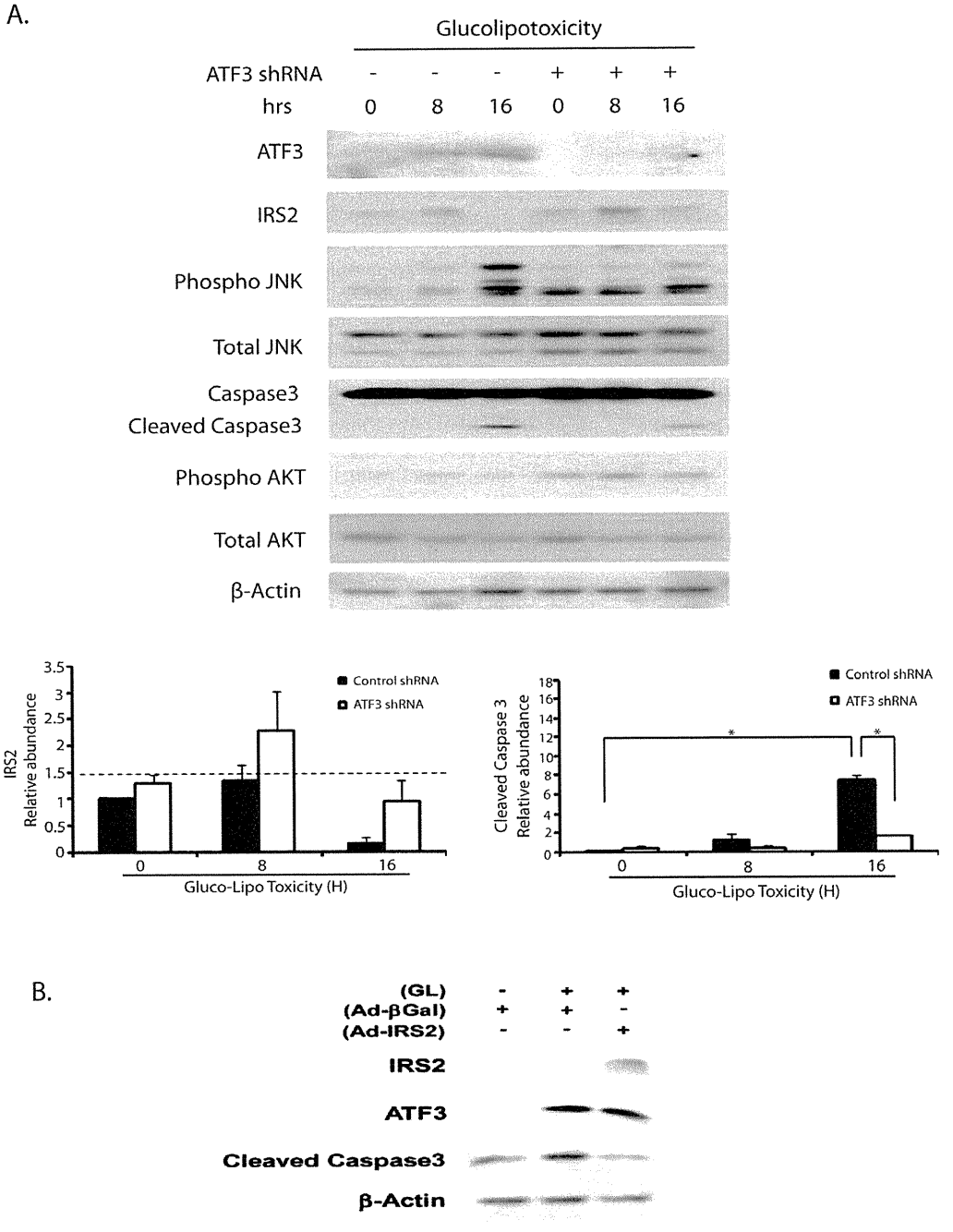

Figure 6. Loss-of-function of ATF3 and gain-of function of IRS2 reduce the effects of glucose and palmitate on apoptosis. (**A**) INS-r3 cells were infected with either control or ATF3 shRNA adenovirus 24-h prior to treatment with 400 μM palmitate+0.5% BSA and 25 mM glucose for the indicated times. Total cell lysates were obtained and subjected to Western blot analysis with antibodies to the indicated proteins. The relative ratio of IRS2 and cleaved Caspase3 expression over β-Actin was quantified by densitometry. The data obtained from three individual experiments are expressed as means ± S.E.M. * $p<0.02$, ** $p<0.012$. (**B**) In a single experiment, primary mouse islets were infected with adenovirus expressing βgal or IRS2 expressing adenovirus prior to treatment with either control 0.5% BSA and 5.5 mM glucose or 400 μM palmitate+0.5% BSA and 25 mM glucose for 72-h. "GL" refers to incubation in 25 mM glucose and 400 μM palmitate. Total cell lysates were subjected to Western blot using antibodies to indicated proteins.
doi:10.1371/journal.pone.0018146.g006

ATF3 induction is dependent on the P38 kinase pathway [15] which is part of signaling transduced by the membrane fatty acid translocase CD36 and a role of CD36, which is induced by glucose, has been proposed in mediating palmitate induced apoptosis of kidney tubular epithelial cell [40]. The role of this pathway in islet cells will need to be explored in future studies.

In the current studies we have shown a correlation among suppression of IRS2 protein levels (Figure 2), ATF3 expression (Figure 3), and resultant induction of apoptosis. The causal relationships among these events were demonstrated by Li. et. al. [14] when insulinoma cells and/or mouse islets were transfected with adenoviruses expressing inducible gain- or loss-of-function of ATF3

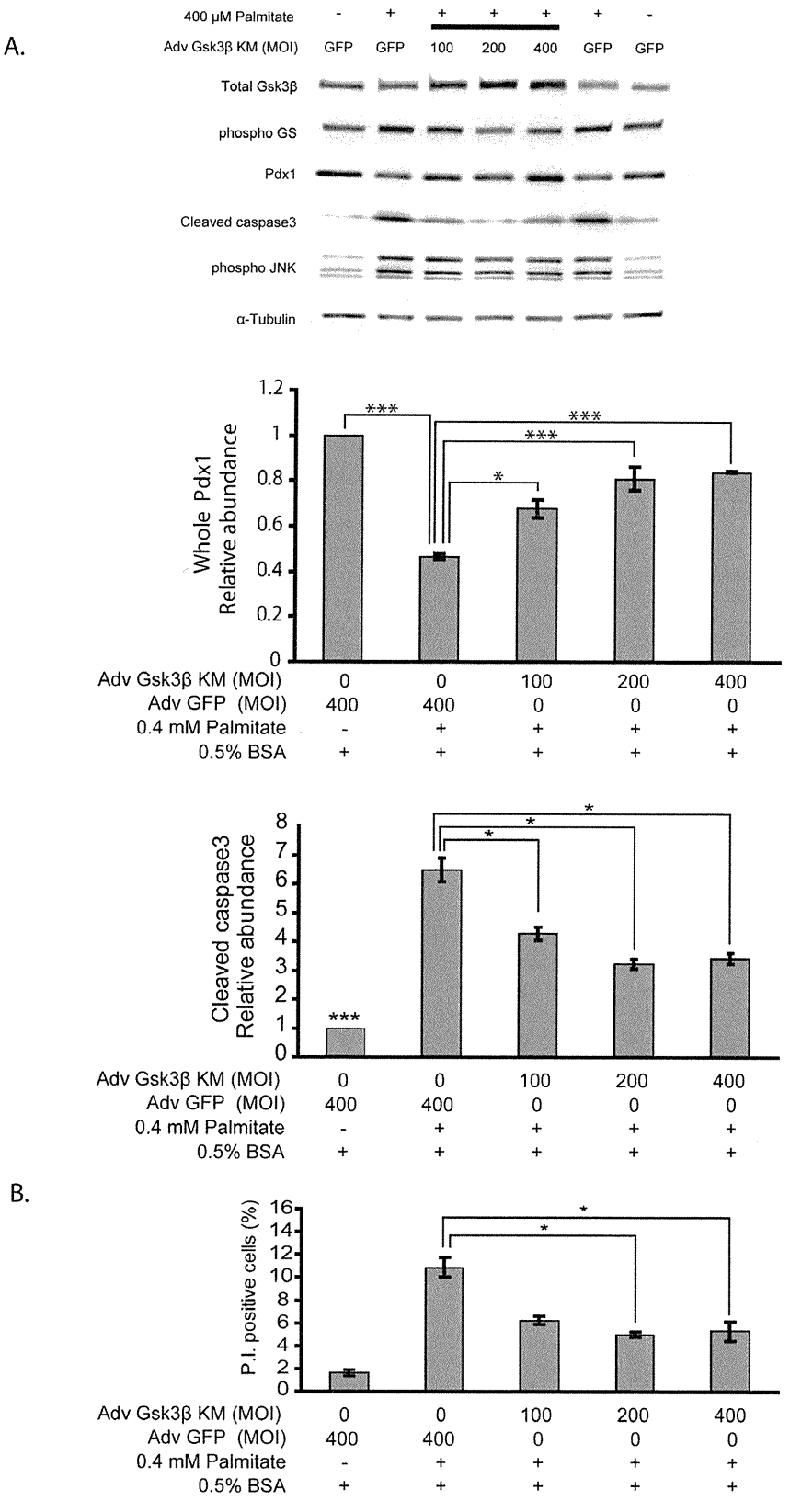

Figure 7. Inhibition of Gsk3β protects against glucose and palmitate-induced apoptosis in MIN6 cells. MIN6 cells were infected with 100, 200, or 400 MOI of adenovirus expressing a catalytically inactive mutant of the human Gsk3β (Adv-Gsk3βKM) or adenovirus expressing GFP (Adv-GFP) 24 hours prior to palmitate treatment. Cells were treated with 25 mM glucose and with either 0.5% BSA or 400 µM PA+0.5% BSA for 24 hours. A GFP control was placed on either end of the blot to facilitate comparison of control and Adv-Gsk3βKM. (**A**) Western blots using the indicated antibodies, with relative expression of Pdx1 normalized over α-Tubulin, and expression levels of cleaved Caspase3 normalized over α-tubulin. (**B**) Percentage of Propidium Iodide incorporation (n = 3, means ± S.E.M., *$p<0.05$, *** $p<0.001$).
doi:10.1371/journal.pone.0018146.g007

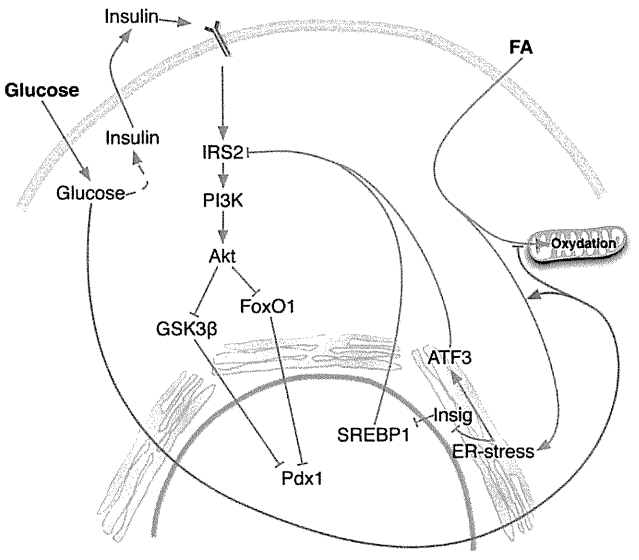

Figure 8. Working diagram illustrating some of the key steps involved in "glucolipotoxicity" of β-cells. High glucose and FFA together result in a vicious negative cycle that ultimately promotes β-cell death. As suggested by our findings, high glucose addition to FFA treated β-cells results in much more activation of SREBP1 than glucose alone. SREBP1 enhances ACC expression with generation of malonyl-CoA which impairs FFA oxidation. This in turn leads to augmented ER stress with further activation of ER-localized SREBP1 as a result of degradation of the anchoring protein Insig1. The excess non-metabolized FFA due to more impairment of FFA oxidation would partition in ER membranes compounding ER stress. In addition to SREBP1, ER stress activates ATF3. Both nuclear SREBP1 and ATF3 result in inhibition of IRS2, with concomitant impairment of insulin signaling, activation of Gsk3β and reduction of Pdx1 leading to apoptosis.
doi:10.1371/journal.pone.0018146.g008

and IRS2. Treatments that induced ATF3 activation and IRS2 suppression included induction of apoptosis by combined treatment of insulinoma cells with γ-interferon, TNF-α, or the ER stress activator thapsigargin. These studies demonstrated that ATF3, like the transcription factor CREB, alters IRS2 expression by binding to the IRS2 promoter. In the current study, we have examined the role of combined glucose and palmitate on this pathway (Figure 6). Transduction with an adenovirus expressing shATF3 significantly reduced this effect, while transduction with AdV-IRS2 ameliorated the apoptotic effect, thus mechanistically linking this pathway.

In this study co-incubation of insulinoma cells with an adenovirus expressing a kinase dead Gsk3β (Adv-Gsk3βKM, Figure 7) along with high glucose and palmitate for 24 hours significantly reduced cleaved Caspase3 and cell death. A previous study in IRS2 null mice had demonstrated that the severe diabetes associated with markedly increased apoptosis and reduced proliferation of islet β-cells was reversed when crossed with Gsk3β haploinsufficient mice [32]. The double knockout was also associated with enhanced expression of Pdx1 in islet β-cells. Like the IRS2 null mice with severe insulin resistance, glucose and FFA treatment of insulinoma cells and primary islets induces a state of insulin resistance. Also like IRS2 null mice on the Gsk3β genetic deficient background, reducing Gsk3β activity with a kinase dead Gsk3β adenovirus restored Pdx1 levels and reduced apoptosis and cell death. These findings emphasize the contribution of impaired insulin receptor substrate signaling in the apoptosis of β-cells treated with glucose and FFA, and the contribution of Gsk3β activity to this process.

A schematic diagram highlights the key concepts implied by our findings (Figure 8). In the insulin resistant subject abnormal metabolism of FFA and glucose result in chronically high levels of both nutrients in the circulation [41]. Under such conditions, the combination of hyperglycemia and FFA has been suggested to be particularly harmful for β-cells leading to so-called glucolipotoxicity [6,42,43]. Our findings suggest that addition of high glucose to FFA treated β-cells results in an escalating negative cycle. Under such conditions activation of the transcription factor SREBP1 leads to enhanced ACC expression with generation of malonyl-CoA (MCC), which impairs FFA oxidation. These in turn lead to ER stress with further activation of SREBP1, ATF3, and impairment of FFA oxidation. The excess unmetabolized FFA would partition in ER membranes compounding ER stress. Additionally nuclear SREBP1 and ATF3 result in inhibition of IRS2, with concomitant impairment of insulin receptor substrate signaling, increase of Gsk3β activity and reduction of Pdx1 leading to apoptosis. Several steps in the cycle shown in Figure 8 may be amenable to therapeutic intervention. These include the impairment of FFA oxidation by glucose, the synergistic effects of glucose and FFA on ER stress, the activation of SREBP1 and its negative effects on insulin signaling, and the downstream mediators of apoptosis that are activated by reduced IRS-signaling involving both Gsk-3β and Fox01.

The results of the current studies illustrate some of the potential mechanisms whereby a combination of high glucose and FFA, as occurs in insulin resistant subjects, may result in eventual destruction of β-cells. However, the ultimate contribution of these mechanisms to the etiology of β-cell failure and diabetes remains unknown and will need to be validated *in vivo*.

Author Contributions

Conceived and designed the experiments: MAP YT YL SCM CCM EBM EZ TH NAA. Performed the experiments: KT YL CMW EZ. Analyzed the data: KT YL SDH SCM CCM EBM YT CJR EZ TH NAA MAP. Contributed reagents/materials/analysis tools: SCM CMW CJR EZ. Wrote the paper: KT YL SDH CCM EBM YT TH NAA MAP.

References

1. Butler AE, Janson J, Bonner-Weir S, Ritzel R, Rizza RA, et al. (2003) Beta-cell deficit and increased beta-cell apoptosis in humans with type 2 diabetes. Diabetes 52: 102–110.
2. Weir GC, Laybutt DR, Kaneto H, Bonner-Weir S, Sharma A (2001) Beta-cell adaptation and decompensation during the progression of diabetes. Diabetes 50 Suppl 1: S154–159.
3. Unger RH (2001) [Maurice Derot Prize 2001. The liporegulator system and disease]. Journ Annu Diabetol Hotel Dieu. pp 129–143.
4. Donath MY, Halban PA (2004) Decreased beta-cell mass in diabetes: significance, mechanisms and therapeutic implications. Diabetologia 47: 581–589.
5. Zhou YP, Grill VE (1994) Long-term exposure of rat pancreatic islets to fatty acids inhibits glucose-induced insulin secretion and biosynthesis through a glucose fatty acid cycle. J Clin Invest 93: 870–876.
6. Poitout V, Robertson RP (2008) Glucolipotoxicity: fuel excess and beta-cell dysfunction. Endocr Rev 29: 351–366.
7. Cnop M (2008) Fatty acids and glucolipotoxicity in the pathogenesis of Type 2 diabetes. Biochem Soc Trans 36: 348–352.
8. Wrede CE, Dickson LM, Lingohr MK, Briaud I, Rhodes CJ (2002) Protein kinase B/Akt prevents fatty acid-induced apoptosis in pancreatic beta-cells (INS-1). J Biol Chem 277: 49676–49684.
9. Kharroubi I, Ladriere L, Cardozo AK, Dogusan Z, Cnop M, et al. (2004) Free fatty acids and cytokines induce pancreatic beta-cell apoptosis by different mechanisms: role of nuclear factor-kappaB and endoplasmic reticulum stress. Endocrinology 145: 5087–5096.
10. Cnop M, Ladriere L, Hekerman P, Ortis F, Cardozo AK, et al. (2007) Selective inhibition of eukaryotic translation initiation factor 2 alpha dephosphorylation potentiates fatty acid-induced endoplasmic reticulum stress and causes pancreatic beta-cell dysfunction and apoptosis. J Biol Chem 282: 3989–3997.
11. Pirot P, Ortis F, Cnop M, Ma Y, Hendershot LM, et al. (2007) Transcriptional regulation of the endoplasmic reticulum stress gene chop in pancreatic insulin-producing cells. Diabetes 56: 1069–1077.

12. Laybutt DR, Preston AM, Akerfeldt MC, Kench JG, Busch AK, et al. (2007) Endoplasmic reticulum stress contributes to beta cell apoptosis in type 2 diabetes. Diabetologia 50: 752–763.
13. Bachar E, Ariav Y, Ketzinel-Gilad M, Cerasi E, Kaiser N, et al. (2009) Glucose amplifies fatty acid-induced endoplasmic reticulum stress in pancreatic beta-cells via activation of mTORC1. PLoS ONE 4: e4954.
14. Li D, Yin X, Zmuda EJ, Wolford CC, Dong X, et al. (2008) The repression of IRS2 gene by ATF3, a stress-inducible gene, contributes to pancreatic beta-cell apoptosis. Diabetes 57: 635–644.
15. Hai T, Hartman MG (2001) The molecular biology and nomenclature of the activating transcription factor/cAMP responsive element binding family of transcription factors: activating transcription factor proteins and homeostasis. Gene 273: 1–11.
16. Martinez SC, Tanabe K, Cras-Meneur C, Abumrad NA, Bernal-Mizrachi E, et al. (2008) Inhibition of Foxo1 protects pancreatic islet beta-cells against fatty acid and endoplasmic reticulum stress-induced apoptosis. Diabetes 57: 846–859.
17. Ishihara H, Asano T, Tsukuda K, Katagiri H, Inukai K, et al. (1993) Pancreatic beta cell line MIN6 exhibits characteristics of glucose metabolism and glucose-stimulated insulin secretion similar to those of normal islets. Diabetologia 36: 1139–1145.
18. Hohmeier HE, Mulder H, Chen G, Henkel-Rieger R, Prentki M, et al. (2000) Isolation of INS-1-derived cell lines with robust ATP-sensitive K+ channel-dependent and -independent glucose-stimulated insulin secretion. Diabetes 49: 424–430.
19. Girish V, Vijayalakshmi A (2004) Affordable image analysis using NIH Image/ImageJ. Indian J Cancer 41: 47.
20. Bernal-Mizrachi E, Fatrai S, Johnson JD, Ohsugi M, Otani K, et al. (2004) Defective insulin secretion and increased susceptibility to experimental diabetes are induced by reduced Akt activity in pancreatic islet beta cells. J Clin Invest 114: 928–936.
21. Finlay D, Patel S, Dickson LM, Shpiro N, Marquez R, et al. (2004) Glycogen synthase kinase-3 regulates IGFBP-1 gene transcription through the thymine-rich insulin response element. BMC Mol Biol 5: 15.
22. Srinivasan S, Bernal-Mizrachi E, Ohsugi M, Permutt MA (2002) Glucose promotes pancreatic islet beta-cell survival through a PI 3-kinase/Akt-signaling pathway. Am J Physiol Endocrinol Metab 283: E784–793.
23. White MF (2002) IRS proteins and the common path to diabetes. Am J Physiol Endocrinol Metab 283: E413–422.
24. Srinivasan S, Ohsugi M, Liu Z, Fatrai S, Bernal-Mizrachi E, et al. (2005) Endoplasmic reticulum stress-induced apoptosis is partly mediated by reduced insulin signaling through phosphatidylinositol 3-kinase/Akt and increased glycogen synthase kinase-3beta in mouse insulinoma cells. Diabetes 54: 968–975.
25. Hartman MG, Lu D, Kim ML, Kociba GJ, Shukri T, et al. (2004) Role for activating transcription factor 3 in stress-induced beta-cell apoptosis. Mol Cell Biol 24: 5721–5732.
26. Ramalho RM, Viana RJ, Low WC, Steer CJ, Rodrigues CM (2008) Bile acids and apoptosis modulation: an emerging role in experimental Alzheimer's disease. Trends Mol Med 14: 54–62.
27. Shimano H (2007) SREBP-1c and TFE3, energy transcription factors that regulate hepatic insulin signaling. J Mol Med 85: 437–444.
28. Goldstein JL, DeBose-Boyd RA, Brown MS (2006) Protein sensors for membrane sterols. Cell 124: 35–46.
29. Kakuma T, Lee Y, Higa M, Wang Z, Pan W, et al. (2000) Leptin, troglitazone, and the expression of sterol regulatory element binding proteins in liver and pancreatic islets. Proc Natl Acad Sci U S A 97: 8536–8541.
30. Takahashi A, Motomura K, Kato T, Yoshikawa T, Nakagawa Y, et al. (2005) Transgenic mice overexpressing nuclear SREBP-1c in pancreatic beta-cells. Diabetes 54: 492–499.
31. Wang H, Kouri G, Wollheim CB (2005) ER stress and SREBP-1 activation are implicated in beta-cell glucolipotoxicity. J Cell Sci 118: 3905–3915.
32. Tanabe K, Liu Z, Patel S, Doble BW, Li L, et al. (2008) Genetic deficiency of glycogen synthase kinase-3beta corrects diabetes in mouse models of insulin resistance. PLoS Biol 6: e37.
33. Cunha DA, Hekerman P, Ladriere L, Bazarra-Castro A, Ortis F, et al. (2008) Initiation and execution of lipotoxic ER stress in pancreatic beta-cells. J Cell Sci 121: 2308–2318.
34. Urano F, Wang X, Bertolotti A, Zhang Y, Chung P, et al. (2000) Coupling of stress in the ER to activation of JNK protein kinases by transmembrane protein kinase IRE1. Science 287: 664–666.
35. Kawamori D, Kaneto H, Nakatani Y, Matsuoka TA, Matsuhisa M, et al. (2006) The forkhead transcription factor Foxo1 bridges the JNK pathway and the transcription factor PDX-1 through its intracellular translocation. J Biol Chem 281: 1091–1098.
36. Lee JN, Ye J (2004) Proteolytic activation of sterol regulatory element-binding protein induced by cellular stress through depletion of Insig-1. J Biol Chem 279: 45257–45265.
37. Lu D, Chen J, Hai T (2007) The regulation of ATF3 gene expression by mitogen-activated protein kinases. Biochem J 401: 559–567.
38. Altomonte J, Richter A, Harbaran S, Suriawinata J, Nakae J, et al. (2003) Inhibition of Foxo1 function is associated with improved fasting glycemia in diabetic mice. Am J Physiol Endocrinol Metab 285: E718–728.
39. Accili D, Arden KC (2004) FoxOs at the crossroads of cellular metabolism, differentiation, and transformation. Cell 117: 421–426.
40. Susztak K, Ciccone E, McCue P, Sharma K, Bottinger EP (2005) Multiple metabolic hits converge on CD36 as novel mediator of tubular epithelial apoptosis in diabetic nephropathy. PLoS Med 2: e45.
41. Paolisso G, Tataranni PA, Foley JE, Bogardus C, Howard BV, et al. (1995) A high concentration of fasting plasma non-esterified fatty acids is a risk factor for the development of NIDDM. Diabetologia 38: 1213–1217.
42. El-Assaad W, Buteau J, Peyot ML, Nolan C, Roduit R, et al. (2003) Saturated fatty acids synergize with elevated glucose to cause pancreatic beta-cell death. Endocrinology 144: 4154–4163.
43. Prentki M, Joly E, El-Assaad W, Roduit R (2002) Malonyl-CoA signaling, lipid partitioning, and glucolipotoxicity: role in beta-cell adaptation and failure in the etiology of diabetes. Diabetes 51 Suppl 3: S405–413.

Int J Hematol (2011) 94:300–302
DOI 10.1007/s12185-011-0918-4

LETTER TO THE EDITOR

Activation of the unfolded protein response in primary acute myeloid leukemia cells

Atsuko Tanimura · Toshiaki Yujiri · Yoshinori Tanaka · Mayumi Tanaka · Noriyuki Mitani · Yukinori Nakamura · Koichi Ariyoshi · Yukio Tanizawa

Received: 8 April 2011 / Revised: 11 August 2011 / Accepted: 11 August 2011 / Published online: 24 August 2011

The unfolded protein response (UPR), which plays an important role in maintaining homeostasis of the endoplasmic reticulum (ER), is known to be activated in various solid tumors [1]. The role of the UPR in different forms of cancer or metastasis remains poorly characterized, and it is unclear whether UPR activation in cancer is due solely to microenvironmental stress, or to other mechanisms. The influence of the UPR on leukemogenesis remains largely uninvestigated. We previously reported that the UPR is activated in Philadelphia (Ph)-positive leukemia cells using cell lines and primary cells from Ph-positive acute lymphoid leukemia (ALL) patients [2]. In the present study, we investigated whether the UPR is activated in another type of acute leukemia, primary acute myeloid leukemia (AML).

We performed real-time reverse transcription-polymerase chain reaction (RT-PCR) focusing on four UPR-related genes to validate the upregulation of the UPR in AML cells: the spliced form of X-box-binding protein 1 (XBP1s), which is a key transcription factor of the UPR; ER-degradation enhancing α-mannosidase-like protein 1 (EDEM1), which is involved in ER-associated degradation; glucose-regulated protein 78 (GRP78), which is an ER chaperone; and C/EBP-homologous protein-10 (CHOP), which is also a transcription factor. We analyzed samples from AML patients [26 bone marrow (BM) and four peripheral blood (PB) samples] and healthy controls (16 BM and 18 PB samples). The collection of mononuclear cells and total RNA extraction was described previously [2]. Total RNA was subjected to reverse transcription with a high-capacity RNA-to-cDNA kit (Applied Biosystems) according to the manufacturer's instructions. Quantitative RT-PCR of the indicated genes was performed using a Power SYBR® PCR Master Mix (Applied Biosystems) with a StepOnePlus™ Real Time PCR System (Applied Biosystems). The primer sequences for each of the human UPR-related genes are as follows: XBP1s, 5′-ggagttaagacagcgcttggg-3′ and 5′-acctgctgcggactcagc-3′; GRP78/BiP, 5′-gagttcttcaatggcaagg-3′ and 5′- ggggacatacatcaagcag-3′; EDEM1, 5′-cagctccaactgcaatcgtgta-3′ and 5′-atctggtcaatctgtcgcatgta-3′; CHOP/GADD153, 5′-gagagagtgttcaagaaggaagtgtatc-3′ and 5′-ccgaaggagaaaggcaatga-3′; β-actin, 5′-tggcaccacaccttctacaatg-3′ and 5′-tctcaaacatgatctgggtcatc-3′. Calculated concentrations were normalized to the expression level of β-actin mRNA. Statistical analyses were performed using Mann–Whitney's U test.

The UPR involves the cleavage of XBP1 mRNA to generate the spliced form XBP1s, which has been shown to be a sensitive marker for the activation of the UPR [3]. We found that the expression of XBP1s mRNA was significantly higher in the AML patients than in the healthy controls in both the BM and PB samples ($P < 0.05$). Furthermore, the expression of GRP78, EDEM1, and CHOP mRNAs was significantly higher in the AML patients than in the healthy controls ($P < 0.05$) (Fig. 1a). The patients' data classified according to the French-American-British classification are shown in Fig. 1b. In the acute promyelocytic leukemia (APL) patients, the expression of GRP78 mRNA was especially higher than in the other AML samples.

A. Tanimura · T. Yujiri · Y. Tanaka · M. Tanaka · N. Mitani · Y. Nakamura · K. Ariyoshi · Y. Tanizawa
Department of Bio-Signal Analysis, Yamaguchi University Graduate School of Medicine, Ube, Japan

T. Yujiri (✉)
Department of Hematopoietic Stem Cell and Leukemia Research, Yamaguchi University School of Medicine, 1-1-1 Minamikogushi, Ube, Yamaguchi 755-8505, Japan
e-mail: yujirit@yamaguchi-u.ac.jp

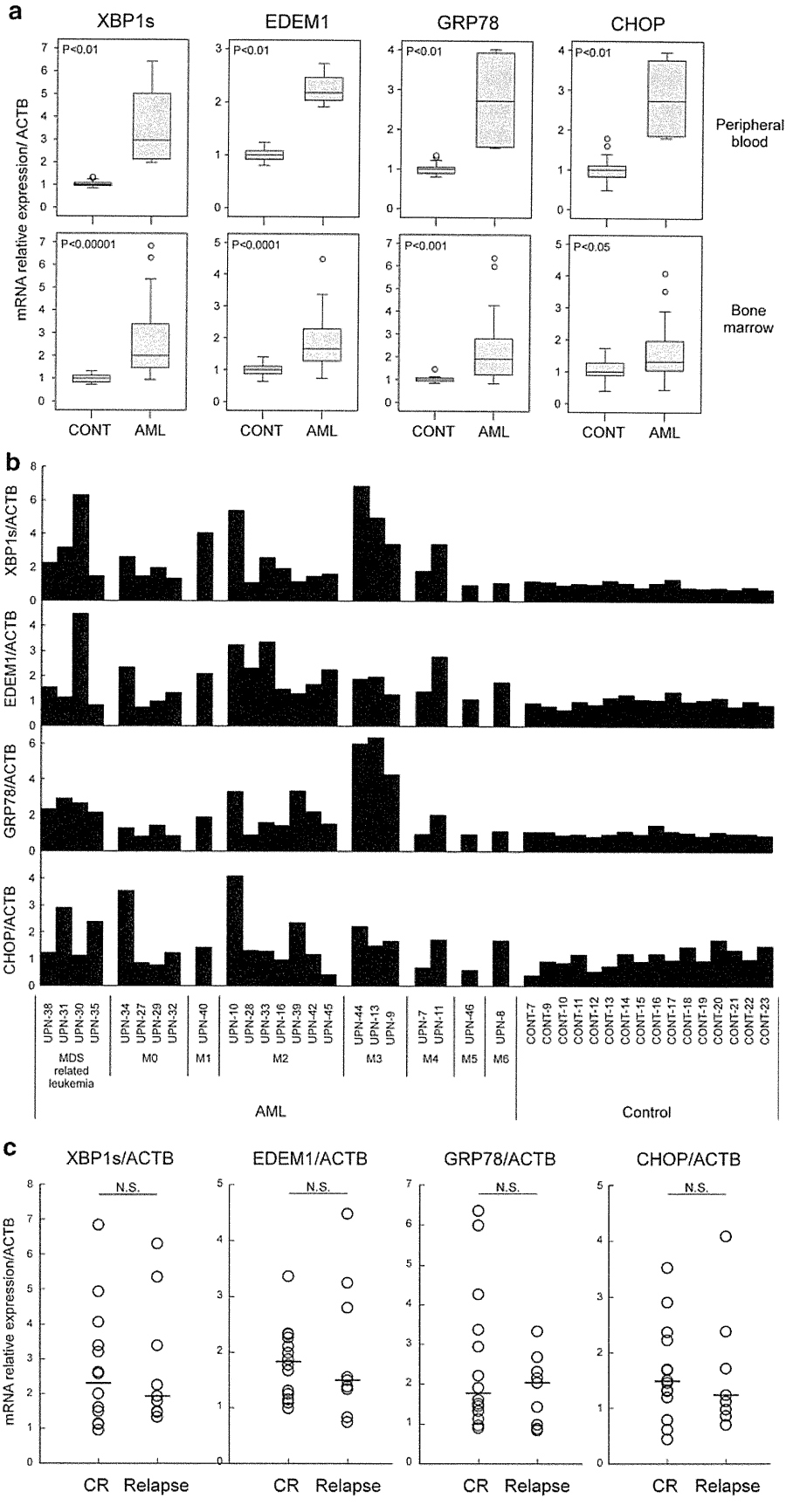

Fig. 1 UPR-related genes are upregulated in bone marrow (BM) and peripheral blood (PB) from acute myeloid leukemia (AML) patients. **a** The expression of XBP1s, EDEM1, GRP78, and CHOP mRNA is significantly upregulated in primary PB (*upper*) and BM (*lower*) AML samples compared to healthy control samples. **b** The expression of the 4 types of mRNA from primary BM samples individually with their diagnosis and the transcript levels after normalization against β-actin (ACTB) in healthy individuals and leukemia patients are shown. **c** Comparison of the expression of the 4 types of mRNA from BM AML samples at the initial visit between the patients with sustained complete response (*CR*) and those who experienced relapse (*Relapse*) (*NS* not significant, P values > 0.1)

The UPR is initially a self-protective response aimed at restoring normal ER function and maintaining cell survival; however, when ER stress is severe or prolonged, it overrides the salvage mechanisms of the initial UPR, leading to apoptosis [4]. Schardt et al. [5] reported UPR activation in AML patients using the expression of XBP1s by gel electrophoresis analysis; AML patients with an activated UPR presented a favorable course of the disease. This was unexpected, as increasing evidence suggests that the UPR is closely associated with cancer cell survival and resistance to anti-cancer treatments. Bagratuni et al. [6] reported that myeloma patients with high XBP1s levels have a poor clinical outcome. Ph-positive ALL patients, a representative leukemia with a poor prognosis, showed especially high expression levels of XBP1s and EDEM1 mRNA compared to Ph-negative ALL patients and control samples in our study (data not shown). In our previous study, we found that the Bcr-Abl fusion protein activated the UPR, which plays an anti-apoptotic role in Ph-positive leukemia cells [2]. We evaluated the treatment response and the expression of the four mRNAs in AML patients at the initial visit, but did not find any correlation ($P > 0.1$) (Fig. 1c). UPR activation did not seem to be a prognostic factor in the present study. Kahn et al. reported that the promyelocytic leukemia (PML)-retinoic acid receptor (RAR) α fusion protein activated the UPR in APL cells. They suggested that PML-RARα induces the accumulation of the nuclear hormone receptor corepressor in the ER, leading to the induction of ER stress and ATF6 processing [7]. We found a relatively higher expression of UPR-related genes in APL patients, indicating that UPR activation is not only a common characteristic in primary AML cells, but a specific translocation product or genetic alteration might also activate the UPR in leukemic cells. AML cells with prognostically favorable or unfavorable karyotypes and gene mutations might show significant alterations on UPR activation. Larger and more intensive studies are required to determine the influence of the UPR on clinical characteristics and leukemogenesis. It would also be interesting to investigate this mechanism for targeting the UPR in leukemic cells from a therapeutic perspective.

References

1. Ma Y, Hendershot LM. The role of the unfolded protein response in tumour development: friend or foe? Nat Rev Cancer. 2004;4:966–77.
2. Tanimura A, Yujiri T, Tanaka Y, Hatanaka M, Mitani N, Nakamura Y, et al. The anti-apoptotic role of the unfolded protein response in Bcr-Abl-positive leukemia cells. Leuk Res. 2009;33:924–8.
3. Lin JH, Li H, Yasumura D, Cohen HR, Zhang C, Panning B, et al. IRE1 signaling affects cell fate during the unfolded protein response. Science. 2007;318:944–9.
4. Xu C, Bailly-Maitre B, Reed JC. Endoplasmic reticulum stress: cell life and death decisions. J Clin Invest. 2005;115:2656–64.
5. Schardt JA, Weber D, Eyholzer M, Mueller BU, Pabst T. Activation of the unfolded protein response is associated with favorable prognosis in acute myeloid leukemia. Clin Cancer Res. 2009;15:3834–41.
6. Bagratuni T, Wu P, Gonzalez de Castro D, Davenport EL, Dickens NJ, Walker BA, et al. XBP1s levels are implicated in the biology and outcome of myeloma mediating different clinical outcomes to thalidomide-based treatments. Blood. 2010;116:250–3.
7. Khan MM, Nomura T, Chiba T, Tanaka K, Yoshida H, Mori K, et al. The fusion oncoprotein PML-RARalpha induces endoplasmic reticulum (ER)-associated degradation of N-CoR and ER stress. J Biol Chem. 2004;279:11814–24.

Circulation
JOURNAL OF THE AMERICAN HEART ASSOCIATION

American Heart Association®
Learn and Live℠

Blockade of the Nuclear Factor-κB Pathway in the Endothelium Prevents Insulin Resistance and Prolongs Life Spans

Yutaka Hasegawa, Tokuo Saito, Takehide Ogihara, Yasushi Ishigaki, Tetsuya Yamada, Junta Imai, Kenji Uno, Junhong Gao, Keizo Kaneko, Tatsuo Shimosawa, Tomoichiro Asano, Toshiro Fujita, Yoshitomo Oka and Hideki Katagiri

Circulation 2012, 125:1122-1133: originally published online February 1, 2012
doi: 10.1161/CIRCULATIONAHA.111.054346
Circulation is published by the American Heart Association. 7272 Greenville Avenue, Dallas, TX 72514
 Print ISSN: 0009-7322. Online ISSN: 1524-4539

Blockade of the Nuclear Factor-κB Pathway in the Endothelium Prevents Insulin Resistance and Prolongs Life Spans

Yutaka Hasegawa, MD, PhD*; Tokuo Saito, MD, PhD*; Takehide Ogihara, MD, PhD; Yasushi Ishigaki, MD, PhD; Tetsuya Yamada, MD, PhD; Junta Imai, MD, PhD; Kenji Uno, MD, PhD; Junhong Gao, MD, PhD; Keizo Kaneko, MD, PhD; Tatsuo Shimosawa, MD, PhD; Tomoichiro Asano, MD, PhD; Toshiro Fujita, MD, PhD; Yoshitomo Oka, MD, PhD; Hideki Katagiri, MD, PhD

Background—Nuclear factor-κB (NF-κB) signaling plays critical roles in physiological and pathological processes such as responses to inflammation and oxidative stress.

Methods and Results—To examine the role of endothelial NF-κB signaling in vivo, we generated transgenic mice expressing dominant-negative IκB under the Tie2 promoter/enhancer (E-DNIκB mice). These mice exhibited functional inhibition of NF-κB signaling specifically in endothelial cells. Although E-DNIκB mice displayed no overt phenotypic changes when young and lean, they were protected from the development of insulin resistance associated with obesity, whether diet- or genetics-induced. Obesity-induced macrophage infiltration into adipose tissue and plasma oxidative stress markers were decreased and blood flow and mitochondrial content in muscle and active-phase locomotor activity were increased in E-DNIκB mice. In addition to inhibition of obesity-related metabolic deteriorations, blockade of endothelial NF-κB signaling prevented age-related insulin resistance and vascular senescence and, notably, prolonged life span. These antiaging phenotypes were also associated with decreased oxidative stress markers, increased muscle blood flow, enhanced active-phase locomotor activity, and aortic upregulation of mitochondrial sirtuin-related proteins.

Conclusions—The endothelium plays important roles in obesity- and age-related disorders through intracellular NF-κB signaling, thereby ultimately affecting life span. Endothelial NF-κB signaling is a potential target for treating the metabolic syndrome and for antiaging strategies. (***Circulation.*** **2012;125:1122-1133.)**

Key Words: inflammation ■ insulin resistance ■ oxidative stress ■ NF-κB

Nuclear factor-kappa B (NF-κB) is a transcription factor regulating the gene expression of numerous cytokines, growth factors, adhesion molecules, and enzymes involved in a variety of pivotal cellular processes, including responses to inflammation and oxidative stress.[1] Without inflammatory stimuli, NF-κB is maintained in the cytoplasm in a nonactivated form by association with an inhibitor subunit, IκB. In response to activating stimuli, including tumor necrosis factor-α (TNF-α), lipopolysaccharide, and other inflammatory cytokines, IκB is phosphorylated by IκB kinase β, resulting in proteolysis of IκB. Consequently, a nuclear recognition site of NF-κB is exposed, and NF-κB is stimulated to move into the nucleus, resulting in mRNA expression of target genes, including inflammatory cytokines and adhesion molecules.[2]

Editorial see p 1081
Clinical Perspective on p 1133

Obesity is characterized by a state of chronic low-grade inflammation.[3] Oxidative stress is also widely recognized as being associated with various obesity-related disorders.[4] Insulin resistance is an important mechanism underlying obesity-related disorders, eg, diabetes mellitus, hyperlipidemia, and hypertension, collectively called the metabolic syndrome.[5,6] In these metabolic states, NF-κB has been implicated in the processes of both inflammatory responses

Received January 12, 2011; accepted December 27, 2011.

From Division of Molecular Metabolism and Diabetes (Y.H., T. Saito, Y.I., J.I., K.U., K.K., Y.O.) and Department of Metabolic Diseases, Center for Metabolic Diseases (T. Saito, T.O., T.Y., J.G., H.K.), Tohoku University Graduate School of Medicine, Sendai; Faculty of Medicine, Department of Clinical Laboratory (T. Shimosawa) and Department of Nephrology and Endocrinology, Faculty of Medicine (T.F.), University of Tokyo, Tokyo; and Department of Medical Science, Graduate School of Medicine, University of Hiroshima, Hiroshima (T.A.), Japan.

*Drs Hasegawa and Saito contributed equally to this article.

The online-only Data Supplement is available with this article at http://circ.ahajournals.org/lookup/suppl/doi:10.1161/CIRCULATIONAHA.111.054346/-/DC1.

Correspondence to Hideki Katagiri, MD, PhD, Department of Metabolic Diseases, Center for Metabolic Diseases, Tohoku University Graduate School of Medicine, 2-1 Seiryo-machi, Aoba-ku, Sendai 980-8575, Japan. E-mail katagiri@med.tohoku.ac.jp

Circulation **is available at http://circ.ahajournals.org** **DOI: 10.1161/CIRCULATIONAHA.111.054346**

and oxidative stress.[7] Indeed, blockade of the NF-κB signaling pathway by systemic administration of high-dose salicylate or global disruption of IκB kinase β reportedly suppresses inflammatory processes associated with insulin resistance in obesity and type 2 diabetes mellitus.[8,9] However, the sites at which the NF-κB signaling pathway plays critical roles in these pathological processes remain to be elucidated.

The endothelium lines the entire vascular system in a single cell layer, forming an interface between vascular structures and blood. In human adults, ≈10 trillion (10^{13}) cells form an almost 1-kg organ. Endothelial cells produce and react to a wide variety of inflammation-related mediators such as cytokines, growth factors, and adhesion molecules.[10] Endothelial injury and dysfunction are involved in the development of many diseases, including vascular diseases and inflammatory disorders.[11,12] In this context, we hypothesized that NF-κB signaling in endothelial cells contributes to obesity-related disorders. Furthermore, insulin resistance and increased oxidative stress also are commonly observed in aged states. Therefore, we also hypothesized that endothelial proinflammatory responses play important roles in age-related disorders, ultimately affecting life span. Here, using the transgenic technique, we show that blockade of the intracellular NF-κB pathway in the endothelium prevents obesity- and age-related insulin resistance and enhances longevity.

Methods

Animals

Animal studies were conducted in accordance with the institutional guidelines for animal experiments at Tohoku University. The mutant cDNA for human IκBα, with alanine substitutions of 2 serine residues (32 and 36), was cloned into a transgenic vector, pSPTg.T2FpAXK, provided by Thomas N. Sato. This vector contains the Tie2 promoter, SV40 polyA signal, and Tie2 minimum enhancer fragment (Figure 1A). E-DNIκB;A^y/+ mice were obtained by mating male KK A^y (A^y/+) mice (Nippon CLEA, Shizuoka, Japan), a genetic model for obesity-diabetes syndrome, and female E-DNIκB mice. E-DNIκB mice were also crossed with endothelial nitric oxide (NO) synthase (eNOS)–deficient ($Nos3^{-/-}$) mice with the C57BL/6J background[13] to generate E-DNIκB;$Nos3^{-/-}$ mice.

Blood analysis, glucose tolerance tests, insulin tolerance tests, histological analysis, oxygen consumption, and locomotor activity were performed as described[14] in the online-only Data Supplement.

Isolation and Culture of Endothelial Cells

Endothelial cells were isolated from murine lung with a MACS separation unit (Miltenyi Biotec, Surry, UK) as previously described.[15] To quantify vascular cell adhesion molecule-1 (VCAM-1) expression, purified endothelial cells were preincubated for 1 hour and then stimulated with or without TNF-α (10 ng/mL) for 4 hours, followed by quantitative reverse-transcriptase polymerase chain reaction analysis.

Hyperinsulinemic-Euglycemic Clamp

Hyperinsulinemic-euglycemic clamp studies were performed as described previously.[16] Details of the method are given in the online-only Data Supplement.

Blood Pressure Measurement

Systolic blood pressure in the conscious state was measured by the indirect tail cuff method with a model MK-2000 BP monitor (Muromachi Kikai, Tokyo, Japan) according to the manufacturer's instructions.[17] At least 6 readings were obtained for each experiment, and a mean value was assigned to each individual mouse.

Muscle Blood Flow Measurement

Muscle blood flow was measured with the fluorescent microsphere method as previously described.[18] Details of the method are given in the online-only Data Supplement.

Histological Analysis

Tissues sections were prepared and analyzed as described in the online-only Data Supplement. Total adipocyte areas were traced manually and analyzed. White adipocyte areas were measured in ≥100 cells per mouse in each group as described previously.[19]

Detection of Cellular Senescence

Cellular senescence was evaluated by senescence-associated β-galactosidase staining. Senescence-associated β-galactosidase was detected with a senescence detection kit (BioVision, Milpitas, CA) as previously described.[20] Senescence-associated β-galactosidase–positive areas were quantified by Easy Access (AD Science Co, Chiba, Japan).

Statistical Analysis

All data are expressed as mean±SEM. Images shown are representative of data from >3 independent experiments. All statistical analyses were performed with Ekuseru-Tokei 2010 statistical software (Social Survey Research Information Co, Ltd, Tokyo, Japan). Normality was tested with the Kolmogorov-Smirnov test. When data were normally distributed, the statistical significance of differences was assessed by 1-way ANOVA. Multiple experimental groups were compared by use of a Bonferroni test. Data were analyzed with nonparametric ANOVA (Kruskal-Wallis) when conformity to a normal distribution was not confirmed. Repeated-measures ANOVA was used to compare data obtained by serial measurements over time between the 2 experimental groups. Survival rates were compared between E-DNIκB mice and control littermates by the Kaplan-Meier method with log-rank tests. In all analyses, values of $P<0.05$ were accepted as statistically significant.

The authors had full access to and take full responsibility for the integrity of the data. All authors have read and agree to the manuscript as written.

Results

Construction of the Transgene and Generation of the E-DNIκB Mice

To block the NF-κB signaling in endothelial cells, we generated transgenic mice (E-DNIκB mice) in which the dominant-negative form of human IκBα (DNIκBα), with alanine substitutions of 2 serine residues (32 and 36), was expressed under the control of the Tie2 enhancer/promoter (Figure 1A). Immunoblotting of lung lysates confirmed the expression of transgene-derived human IκBα, ie, DNIκBα, with a slightly higher molecular weight than the murine, ie, endogenous, IκBα protein (Figure 1B). Transgene expression was apparent in the lung, in which the endothelium is abundant, but was only faintly detectable in other tissues such as the liver, pancreas, muscle, and adipose tissue (Figure 1B). In addition, endogenous IκBα proteins were degraded whereas DNIκBα remained essentially intact without degradation after TNF-α stimulation (Figure 1C). Immunostaining of lung tissue revealed that movement of NF-κB to the nucleus in response to TNF-α stimulation was markedly inhibited by DNIκBα expression (Figure 1D).

To further confirm the functional inhibition of endothelial NF-κB signaling, we isolated endothelial cells from murine

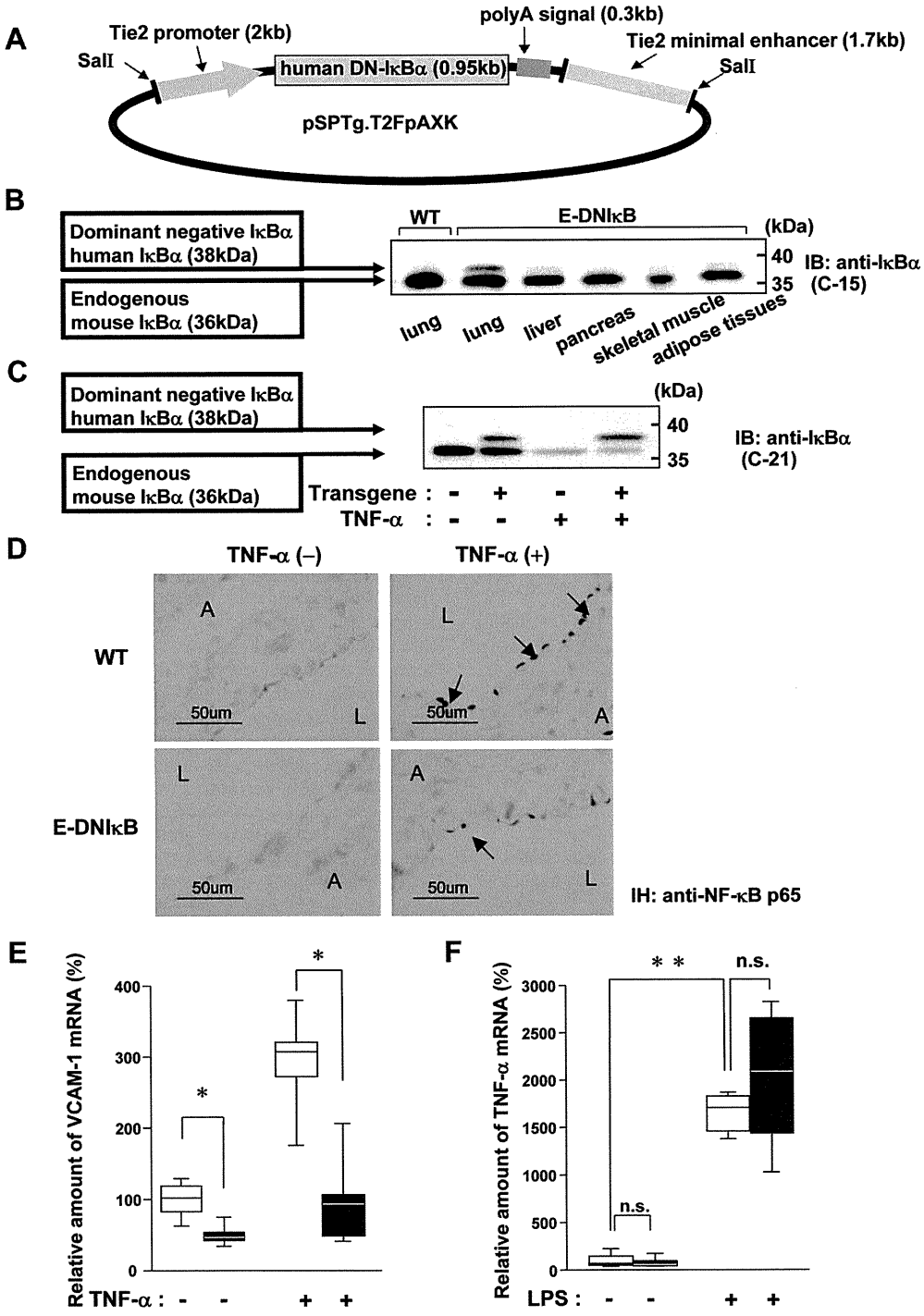

Figure 1. Generation of endothelial dominant-negative IκBα transgenic (E-DNIκB) mice. **A**, The construct of the transgene for generating E-DNIκB mice. **B**, Extracts of various tissues, as indicated, obtained from control and E-DNIκB mice were immunoblotted with anti-IκBα antibody. Exogenous (human) IκBα has a slightly higher molecular weight than endogenous (murine) IκBα. WT indicates wild type. **C**, Lung extracts of nontransgenic (control) and E-DNIκB mice were obtained 30 minutes after injection of tumor necrosis factor-α (TNF-α; 25 μg/kg), followed by immunoblotting with anti-IκBα antibody. **D**, Sections of thoracic aortas obtained from control and E-DNIκB mice were immunostained with anti-p65 (nuclear factor-κB [NF-κB] subunit) antibody. L indicates lumen; A, adventitia. Arrows indicate endothelial nuclei. **E**, Endothelial cells were isolated from lungs of control (white bars) and E-DNIκB (black bars) mice (n=6 per group) by use of a MACS separation unit. Purified endothelial cells were stimulated with or without TNF-α (10 ng/mL) for 4 hours, followed by analysis of vascular cell adhesion molecule-1 (VCAM-1) expression by quantitative reverse-transcriptase polymerase chain reaction (RT-PCR). **F**, Circulating blood cells from control (white bars) and E-DNIκB (black bars) mice (n=5 per group) were stimulated with or without lipopolysaccharide (100 ng/mL) for 3 hours, followed by analysis of TNF-α expression by quantitative RT-PCR analysis. In **E** and **F**, the relative amounts of mRNA were calculated with β-actin mRNA as the invariant control. Data are presented as mean±SEM. *$P<0.05$, **$P<0.01$ by 1-way ANOVA and Kruskal-Wallis tests.

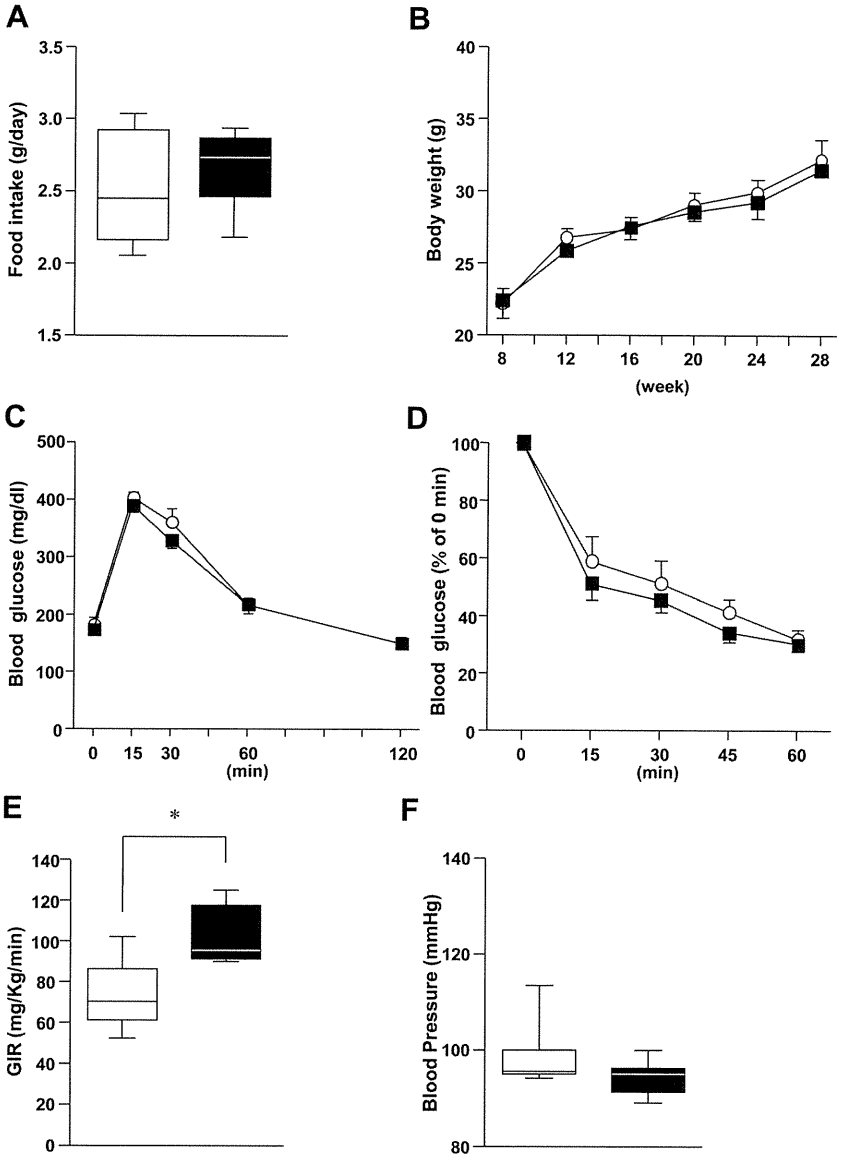

Figure 2. Young endothelial dominant-negative IκBα transgenic (E-DNIκB) mice showed no apparent phenotypic differences. **A**, Control (white bars) and E-DNIκB (black bars) mice were maintained on a normal chow diet, and food intake was measured at 8 weeks of age. **B**, Body weights of control (○) and E-DNIκB (■) mice maintained on a normal chow diet were measured weekly from 8 to 28 weeks of age. **C**, Glucose tolerance tests were performed with a peritoneal glucose load (2 g/kg body weight) after a 10-hour fast at 8 weeks of age. **D**, Insulin tolerance tests were performed in an ad libitum–fed state. Data are expressed as percentages of blood glucose levels immediately before intraperitoneal insulin loading (0.25 U/kg body weight). **E**, Hyperinsulinemic-euglycemic clamp tests were performed in control (white bars, n=4) and E-DNIκB (black bars, n=4) mice at 8 weeks of age, and glucose infusion rate (GIR) was calculated. **F**, Systolic blood pressures of control and E-DNIκB mice were measured at 8 weeks of age. Data are presented as mean±SEM. n=5 in control and n=6 in E-DNIκB mice. *$P<0.05$ by 1-way and repeated-measures ANOVA.

lung and analyzed the expression of VCAM-1, a target gene of NF-κB.[21] In isolated endothelial cells from wild-type mice, TNF-α upregulated VCAM-1 expression, whereas basal and TNF-α–induced VCAM-1 expression was markedly inhibited in isolated endothelial cells from E-DNIκB mice (Figure 1E). In contrast, in circulating cells from E-DNIκB mice, neither basal nor lipopolysaccharide-induced TNF-α expression was suppressed (Figure 1F). These findings demonstrate that NF-κB signaling is functionally blocked specifically in endothelial cells of the E-DNIκB mice used in this study.

Young E-DNIκB Mice Showed No Apparent Phenotypic Differences Compared With Control Mice

First, we analyzed glucose metabolism in these mice on a normal chow diet at 8 weeks of age. Food intakes (Figure 2A) and body weights (Figure 2B) were similar in E-DNIκB mice and their wild-type littermate controls. Glucose tolerance tests revealed no significant differences in blood glucose levels before and after glucose loading between these 2 groups (Figure 2C). In addition, blood glucose levels on insulin tolerance tests did not differ significantly between these 2 groups (Figure 2D). In contrast, a hyperinsulinemic-euglycemic clamp study, a more sensitive procedure for estimating insulin sensitivity, showed increased glucose infusion rates in E-DNIκB mice (Figure 2E). Because hyperinsulinemia during the clamp procedure suppresses hepatic glucose production, these findings indicate slight improvement of insulin sensitivity in insulin-responsive tissues, mainly muscle. Furthermore, systolic blood pressure was also similar in these 2 groups (Figure 2F). Thus, although young and on a normal chow diet, E-DNIκB mice showed no apparent phenotypic differences from control mice, except for slightly improved insulin sensitivity.

E-DNIκB Mice Were Protected From Obesity-Induced Insulin Resistance

We next analyzed the effects of endothelial NF-κB signaling blockade on glucose metabolism and insulin sensitivity in

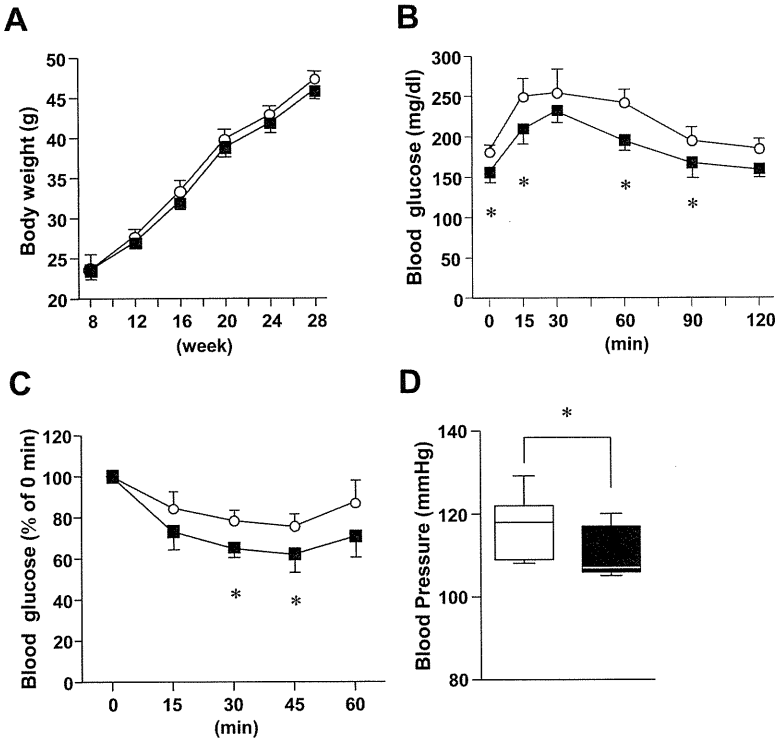

Figure 3. Endothelial dominant-negative IκBα transgenic (E-DNIκB) mice are protected from high-fat diet–induced obesity and insulin resistance. **A**, Body weights of control (○) and E-DNIκB (■) mice maintained on a high-fat diet were measured weekly from 8 to 28 weeks of age. **B**, Glucose tolerance tests were performed with a peritoneal glucose load (0.5 g/kg body weight) after a 10-hour fast in mice maintained on a high-fat diet at 28 weeks of age. **C**, Insulin tolerance tests were performed in an ad libitum–fed state. Data are expressed as percentages of blood glucose levels immediately before intraperitoneal insulin loading (0.8 U/kg body weight) in mice maintained on a high-fat diet at 28 weeks of age. **D**, Systolic blood pressures of control (white bars) and E-DNIκB (black bars) mice maintained on a high-fat diet at 24 to 28 weeks of age. Data are presented as mean±SEM. n=6 in control and n=7 in E-DNIκB mice. *$P<0.05$ by 1-way and repeated-measures ANOVAs.

states of obesity. First, E-DNIκB mice with the C57BL/6J background were placed on a high-fat diet starting from 8 weeks of age. Body weights were similarly increased in E-DNIκB mice and their wild-type littermate controls (Figure 3A). However, after 20 weeks of high-fat loading, differences in glucose tolerance and insulin sensitivity became evident. Glucose and insulin tolerance tests revealed that blockade of endothelial NF-κB signaling significantly protected these mice from the development of glucose intolerance (Figure 3B) and insulin resistance (Figure 3C). Furthermore, systolic blood pressure was significantly lower in E-DNIκB mice (Figure 3D). These findings indicate that inhibition of endothelial NF-κB signaling prevents obesity-induced disorders such as insulin resistance, glucose intolerance, and hypertension.

The prevention of insulin resistance and hypertension achieved by inhibiting endothelial NF-κB signaling was observed in genetically obese ($A^y/+$) mice in earlier periods. Body weights were slightly lower in E-DNIκB;$A^y/+$ than in control littermate $A^y/+$ mice at 16 weeks of age (Figure I in the online-only Data Supplement). Glucose (Figure 4A) and insulin (Figure 4B) tolerance tests revealed markedly better glucose tolerance and insulin sensitivity with blockade of endothelial NF-κB signaling. In contrast, hepatic expression of gluconeogenic genes, phosphoenolpyruvate carboxykinase, and glucose-6-phosphatase did not differ significantly between the 2 groups (Figure II in the online-only Data Supplement), suggesting that muscle is the major tissue responsible for improvement of insulin sensitivity achieved by blockade of endothelial NF-κB signaling. Systolic blood pressure was also significantly lower in E-DNIκB;$A^y/+$ mice than in $A^y/+$ littermates (Figure 4C). In addition, aortic expression of adhesion molecules such as VCAM-1 and E-selectin was decreased in E-DNIκB;$A^y/+$ mice (Figure 4D). Simultaneously, eNOS expression was significantly increased (Figure 4D), which may have contributed to the lower blood pressures.

Obesity-Associated Macrophage Infiltration Into Adipose Tissue Was Markedly Inhibited in E-DNIκB Mice

Obesity is a chronic state of low-grade inflammation leading to insulin resistance and oxidative stress. Macrophage infiltration into white adipose tissue reportedly contributes to the underlying mechanism.[22,23] Therefore, we histologically analyzed white adipose tissue, an important site of obesity-related inflammation. The adipocyte sizes and weights of epididymal fat tissue were smaller in E-DNIκB;$A^y/+$ mice than in control $A^y/+$ littermates, whereas liver weights did not differ significantly (Figure 4E and Figure I in the online-only Data Supplement). These findings suggest that less adiposity contributes to the better glucose tolerance in E-DNIκB;$A^y/+$ mice. Although immunohistochemical staining with antibodies against MOMA-2, a macrophage marker, revealed massive infiltration of macrophages into adipose tissue in $A^y/+$ littermates, macrophage infiltration was markedly inhibited by endothelial blockade of NF-κB signaling (Figure 4E). The inhibition of macrophage infiltration was quantitatively confirmed by reverse-transcriptase polymerase chain reaction. Expression of F4/80 and inducible NO synthase was significantly lower in adipose tissues of E-DNIκB;$A^y/+$ mice than in those of control littermate $A^y/+$ mice (Figure 4F). These findings indicate that endothelial NF-κB signaling is involved in obesity-induced macrophage infiltration into adipose tissue. In addition, E-selectin expression was significantly decreased and VCAM-1 and intercel-

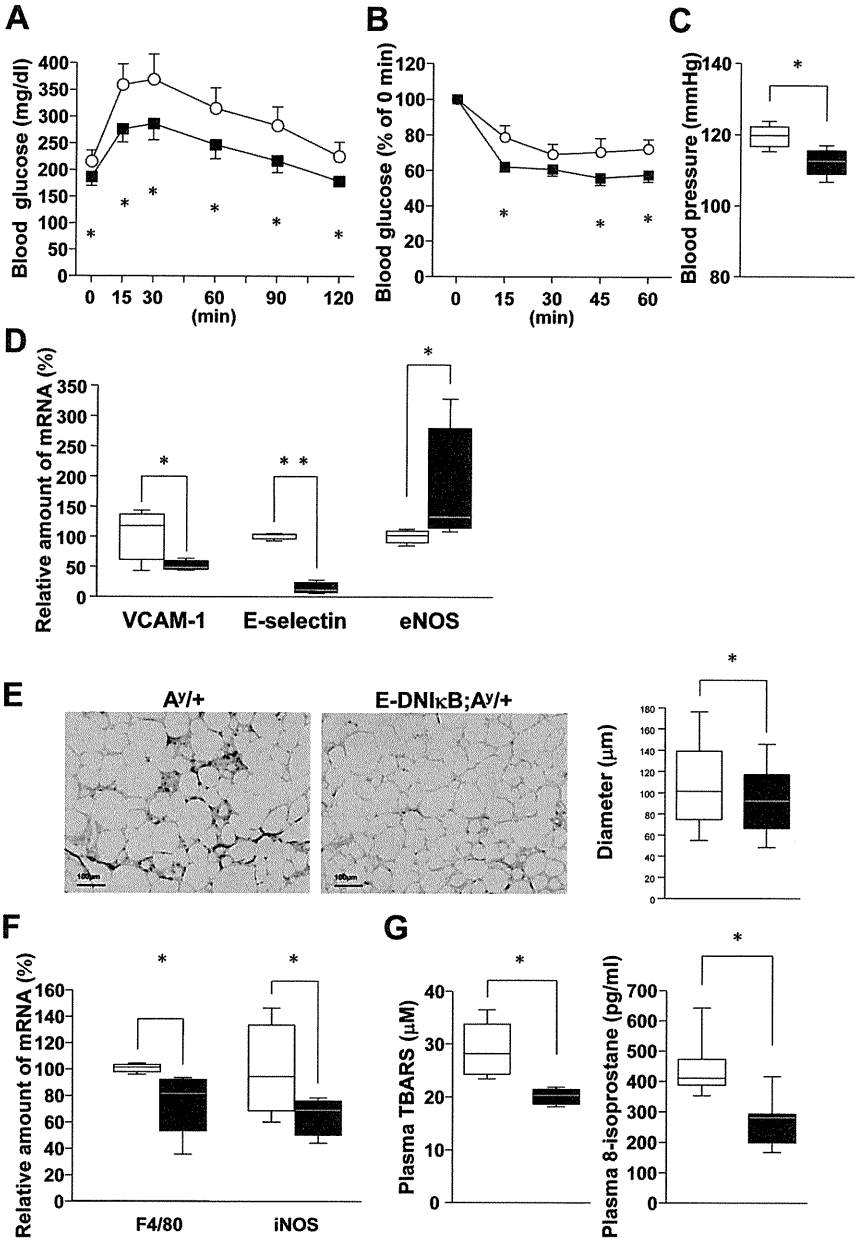

Figure 4. Blockade of endothelial nuclear factor-κB (NF-κB) signaling prevented adipose macrophage infiltration in genetically obese mice. **A**, Male KK A^y (A^y/+) control mice (○) and endothelial dominant-negative IκBα transgenic mice mated with male KK A^y (E-DNIκB;A^y/+; ■) received glucose tolerance tests with a peritoneal glucose load (0.5 g/kg body weight) after a 10-hour fast at 16 weeks of age. **B**, Insulin tolerance tests were performed in an ad libitum–fed state at 16 weeks of age. Data are expressed as percentages of blood glucose levels immediately before intraperitoneal insulin loading (2.5 U/kg body weight). **C**, Systolic blood pressures were measured in A^y/+ control (white bars) and E-DNIκB;A^y/+ (black bars) mice at 16 weeks of age. **D**, Aortic gene expression of vascular cell adhesion molecule-1 (VCAM-1), E-selectin, and endothelial nitric oxide synthase (eNOS) was analyzed in A^y/+ control and E-DNIκB;A^y/+ mice at 16 weeks of age by reverse-transcriptase polymerase chain reaction (RT-PCR). **E**, Epididymal fat from A^y/+ control and E-DNIκB;A^y/+ mice were immunostained with anti-MOMA2 antibody (left). Cell diameters were measured (right). **F**, Gene expression of macrophage markers in epididymal fat was analyzed in A^y/+ control and E-DNIκB;A^y/+ mice by RT-PCR. In **D** and **F**, the relative amounts of mRNA were calculated with β-actin mRNA as the invariant control. **G**, Plasma concentrations of the oxidative stress markers thiobarbituric acid–reactive substance (TBARS) and 8-isoprostane were measured in A^y/+ control and E-DNIκB;A^y/+ mice. Data are presented as mean±SEM. n=5 in A^y/+ control and n=7 in E-DNIκB;A^y/+ mice. *$P<0.05$ by 1-way repeated-measures ANOVAs and Kruskal-Wallis tests.

lular adhesion molecule-1 tended to be downregulated in adipose tissues of E-DNIκB;A^y/+ mice, whereas angiogenesis markers such as Tie2 and vascular endothelial growth factor did not differ (Figure III in the online-only Data Supplement). Thus, suppression of endothelial expression of adhesion molecules might be involved in the decrease in macrophage infiltration into adipose tissue observed in E-DNIκB;A^y/+ mice.

Plasma leptin, TNF-α, and monocyte chemoattractant protein-1 tended to be lower whereas adiponectin was significantly higher in E-DNIκB;A^y/+ mice than in A^y/+ littermates (Figure IV in the online-only Data Supplement). Furthermore, plasma levels of the oxidative stress markers thiobarbituric acid–reactive substance and 8-isoprostane were significantly lower in E-DNIκB;A^y/+ mice than in A^y/+ littermates (Figure 4G). Aortic expression of the antioxidant enzymes manganese superoxide dismutase and glutathione peroxidase was significantly suppressed in E-DNIκB;A^y/+ mice (Figure V in the online-only Data Supplement), suggesting amelioration of oxidative stress in vascular cells. Taken together, these observations indicate that endothelial NF-κB signaling is involved in obesity-associated inflammation and oxidative stress.

Blood Flow and Mitochondrial Contents Were Increased in Muscles of E-DNIκB;A^y/+ Mice

Endothelial adhesion molecule expression is involved in the leukocyte-endothelium interaction, which reportedly affects the microcirculation.[24] In addition, endothelium-derived NO is widely recognized as a major vasodilator[25] that modulates mitochondrial biogenesis.[26] Because endothelial blockade of NF-κB signaling decreased and increased aortic expression of vascular adhesion molecules and eNOS, respectively (Figure 4D), we first measured blood flow in muscle, a major

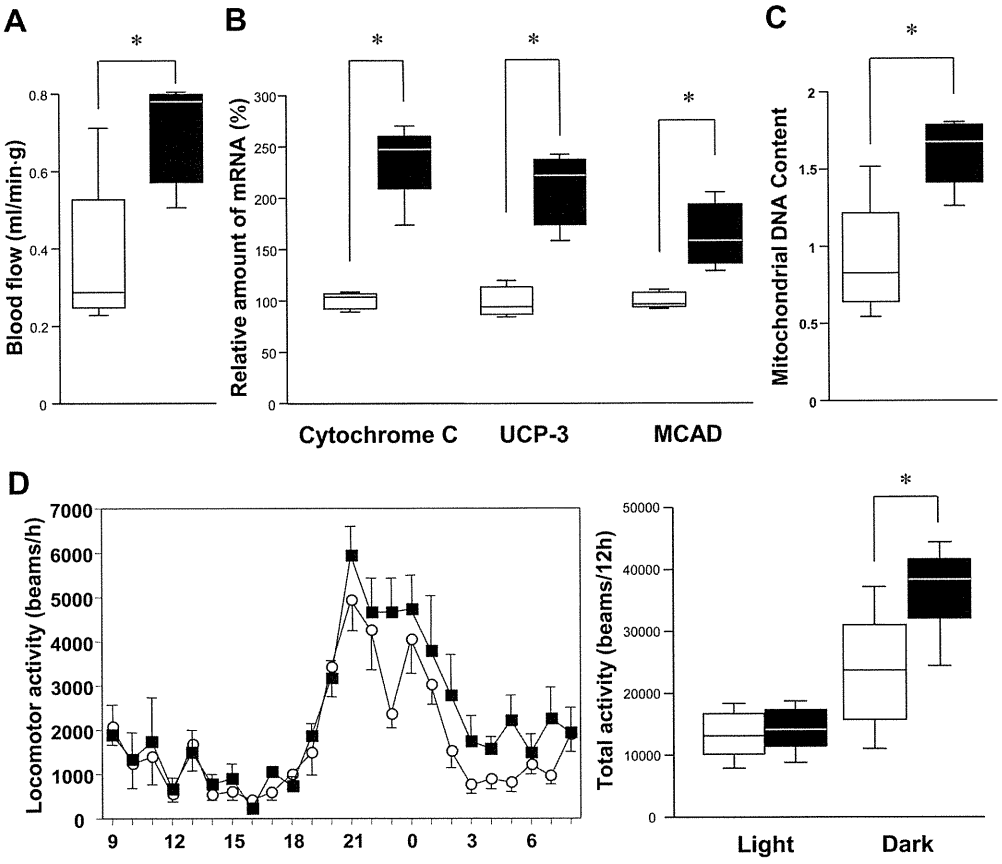

Figure 5. Blood flow and mitochondrial contents were increased in muscles of endothelial dominant-negative IκBα transgenic mice mated with male KK A^y (E-DNIκB;A^y/+) mice. **A**, Gastrocnemius muscle blood flows of 16-week-old A^y/+ control (white bars, n=4) and E-DNIκB;A^y/+ (black bars, n=4) mice were measured with the fluorescent microsphere method. **B**, Gene expression of mitochondrial proteins in muscle was analyzed in A^y/+ control and E-DNIκB;A^y/+ mice by reverse-transcriptase polymerase chain reaction. The relative amounts of mRNA were calculated with α-actin mRNA as the invariant control. UCP-3 indicates uncoupling protein-3; MCAD, medium-chain acyl-CoA dehydrogenase. **C**, Total DNA was extracted from gastrocnemius muscles of A^y/+ control and E-DNIκB;A^y/+ mice, and mitochondrial DNA contents were measured with a sequence detection system. In **B** and **C**, the relative amounts of mRNA were calculated with α-actin mRNA as the invariant control. n=5 in A^y/+ control and n=7 in E-DNIκB;A^y/+ mice. **D**, Locomotor activities at 20 to 24 weeks of age of A^y/+ control (○; n=4) and E-DNIκB;A^y/+ (■; n=4) mice (left). Estimated activities in 12-hour light and dark periods (right) were calculated. Data are presented as mean±SEM. *P<0.05 by 1-way ANOVA.

insulin-sensitive tissue, using the fluorescent microsphere method.[18,27] Blockade of endothelial NF-κB signaling significantly increased blood flow in the muscles of A^y/+ mice (Figure 5A), suggesting involvement in the prevention of obesity-induced insulin resistance. Next, we examined mitochondrial protein expression and mitochondrial DNA contents. Mitochondrial proteins such as cytochrome c, uncoupling protein-3, and medium-chain acyl-CoA dehydrogenase were upregulated in muscles of E-DNIκB;A^y/+ mice compared with A^y/+ littermate controls (Figure 5B). Mitochondrial DNA contents were significantly higher in muscles of E-DNIκB;A^y/+ mice (Figure 5C). These findings indicate that blockade of endothelial NF-κB signaling enhances mitochondrial biogenesis in muscle.

Then, we assessed whether locomotor activity was affected by blockade of endothelial NF-κB signaling. Interestingly, E-DNIκB mice exhibited significant increments in locomotor activity during the 12-hour dark phase, whereas locomotor activities did not differ during the 12-hour light phase (Figure 5D). Compatible with this, oxygen consumption was also increased in E-DNIκB mice during the dark phase but unchanged in the light phase (Figure VI in the online-only Data Supplement). Because muscle blood flow[28] and mitochondrial function[29] are reportedly involved in insulin sensitivity, these enhancements associated with increased locomotor activity may underlie the protection from insulin resistance in response to blockade of endothelial NF-κB signaling.

E-DNIκB Mice Were Protected From Age-Related Insulin Resistance and Blood Pressure Elevation

Insulin resistance, elevated blood pressure, and increased oxidative stress, which were prevented in obese E-DNIκB mice, are also commonly observed in aged states. Therefore, we next examined the effects of endothelial NF-κB blockade on age-related metabolic deteriorations and vascular senescence using 50-week-old E-DNIκB mice on a standard chow diet. Food intakes were similar (Figure VIIA in the online-only Data Supplement), but body weights were slightly lower in aged E-DNIκB mice than in wild-type littermates (Figure VIIB in the online-only Data Supplement). Blood glucose levels after glucose loading tended to